JOURNAL OF THE AERONAUTICAL SCIENCES

VOLUME 10 MAY, 1943 NUMBER 5

Bending Strength in the Plastic Range

FRANK P. COZZONE*

Lockheed Aircraft Corporation

ABSTRACT

The conventional linear distribution of stress in a section subjected to bending in the plastic range, as usually represented by the classical my/I formula, has been replaced by a simple trapezoidal distribution that varies with the applied bending moment. This latter distribution approximates the distribution based on the actual stress-strain characteristics of the material and the shape of the cross section.

A method has been developed for use throughout the elastic and plastic range of bending which covers the following points: (1) the resisting moment of any cross section corresponding to any extreme fiber stress up to the ultimate stress of the material; (2) the corresponding stress distribution over the entire cross section; (3) the corresponding shear distribution; (4) the effects of local crippling; (5) complex bending; and (6) the combined effects of axial load and bending.

SYMBOLS USED

Main (as distinguished from subscript)

- A = area between fiber in question and the extreme fiber
- α = angle the neutral axis makes with respect to the X axis
- b = maximum width of the section
- β = angle the moment vector makes with respect to the X axis
- c = perpendicular distance from a principal axis to the extreme fiber
- e = unit strain
- f = applied stress
- F = allowable stress
- φ = angle the principal X' axis makes with the X axis
- j = an additional (multiplying) factor of safety
- k = section factor
- m = applied moment
- M = allowable moment
- P = normal load on portion of cross section
- Q = static (first) moment, about the neutral axis, of the area between the fiber in question and the extreme fiber
- R = rate of change of trapezoidal stress intercept with respect to the stress of the extreme fiber; or stress ratio
- S = shear load
- x, y = distances measured parallel to the X and Y axes
- X, Y = mutually perpendicular axes
- X', Y' = principal axes
- z = width of section at distance y from the neutral axis

Subscript

- a = due to axial or direct load
- b = due to conventional bending
- d = for a diamond type of cross section
- h = for an hour-glass type of cross section
- L = due to limit or applied load
- m = maximum
- n = due to normal or conventional practice
- o = minimum
- r = for a rectangular type of cross section; or resultant
- t = tensile or total
- u = ultimate
- x = about X axis
- y = about Y axis; or yield; or fiber at distance y from the neutral axis
- x' = about X' axis
- y' = about Y' axis

INTRODUCTION

THE CLASSIC BENDING THEORY is based on the assumption that plane sections before bending remain plane after bending. Since, within the elastic range, stress is proportional to strain, it follows that the stress distribution over the cross section will be linear, varying from zero at the neutral axis to a maximum at the extreme fiber. This distribution is expressed mathematically for a symmetric cross section subjected to simple bending by the conventional formula

$$f_b = my/I \qquad (1)$$

where

- f_b = bending stress at a fiber that is located at a distance y from the neutral axis
- m = the applied moment (lower case used to differentiate applied moment m from allowable moment M)
- I = the moment of inertia about the axis of bending

Presented at the Structures Session, Eleventh Annual Meeting, I.Ae.S., New York, January 25–29, 1943.

* Stress Methods Group Engineer.

When, on the other hand, the extreme fiber stress exceeds the proportional limit stress of the material, the stress distribution over the cross section is no longer linear but tends to follow the stress-strain characteristics of the material.[1] Consequently, the conventional formula for linear bending stress distribution no longer applies. It has been standard aircraft practice, in such cases, to use a "form factor" to indicate the amount by which the allowable ultimate stress of the material could be considered to be increased in order to apply the conventional $f_b = my/I$ formula.

The use of this simple expedient of a form factor necessitates having available the form factors for all the various shapes of cross sections commonly encountered in practice. Such form factors for round tubes have been incorporated in the "Bending Modulus of Rupture Curves for Round Chrome Molybdenum Steel Tubing."[2] Form factors for sections other than round are not available to the average structural engineer. In view of this lack of material, it was proposed to make a further study of form factors for various I-type, channel-type, and round tubular types of cross sections. Simple bending tests were made on such sections, and the data[3] pertinent to this article are included in the Appendix.

The current "form factor" method of accounting for the effects of bending in the plastic range is subject to the following limitations:

(1) The physical significance of the plastic bending phenomenon is lost by the use of a fictitious stress greater than the allowable ultimate stress F_{tu} of the material.

(2) In many cases the full advantage of the form factor effect at ultimate loads cannot be realized since the yield strength criteria must also be met, particularly in aircraft work. Therefore, yield form factors as well as ultimate form factors should be made available.

(3) The stress distribution across the entire cross section is fictitious and, therefore, local crippling effects cannot be taken care of unless a sufficient number of tests are run on various sections of varying wall thickness. (The bending modulus of rupture curves for round tubes of various D/t values include this "local crippling" effect.[2])

(4) In order to include the effect of material properties, a complete set of form factors would have to be made available for each material.

To remove the above limitations it was decided to abandon the conventional form factor theory and evolve another method for handling the plastic bending phenomenon. The use of a bending stress distribution based on the exact stress-strain characteristics of the material was considered but was found to be impractical because of the difficulty of expressing the stress-strain relationship mathematically. Beilschmidt,[4] however, has approximated this relationship by expressing stress f as a function of some power of strain e, ($f = ae^n$). This method, however, was also limited by the mathematical difficulties encountered in applying it to typical problems.

With the idea of utilizing, whenever possible, the common physical properties of a cross section, a trapezoidal distribution approximating the actual stress-strain distribution was found to give a practical solution. The trapezoidal distribution was varied, of course, depending on the extreme fiber stress involved.

A formula was developed to determine the moment of resistance offered by a cross section subjected to any bending moment m. The corresponding formula for shear distribution was also developed.

In order to account for the effect of material properties, curves enabling the designer to account for plastic bending phenomena were developed for each of various materials commonly used in aircraft practice.

A discussion of the proposed method of handling local crippling, complex bending, and combined axial load and bending is included, together with the respective limitations of the proposed method.

Moment of Resistance of a Section Subjected to Bending

Linear or Triangular Stress Distribution

The stress-strain curve may be thought of as a stress distribution curve if the vertical axis is assumed to be the neutral axis.

Fig. 1(a) shows a typical stress-strain curve in which the strain of the extreme fiber e_c corresponds to a stress f_b which is below the proportional limit of the material. The equivalent stress distribution is shown on section A-A of Fig. 1(b).

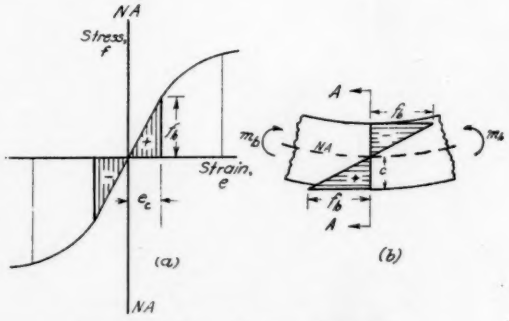

Fig. 1. Triangular stress distribution.

The moment of resistance m_b of the section subjected to bending may be expressed as

$$m_b = f_b(I/c) \qquad (2)$$

Subscript b designates a triangular distribution; f_b is the corresponding extreme fiber stress; and I/c is the conventional section modulus.

Constant or Rectangular Stress Distribution

If a stress-strain curve of a material were as shown in Fig. 2(a), the shaded area could be thought of as the stress distribution. The equivalent stress distribution is shown on section A-A of Fig. 2(b).

The moment of resistance m_r of the section subjected to bending may be expressed approximately as

$$m_r = 2f_rQ_m \tag{3}$$

Subscript r designates a rectangular distribution; f_r is the corresponding extreme fiber stress; and Q_m is the maximum static moment of area (i.e., the first moment about the neutral axis, of the entire area between the neutral axis and the extreme fiber).

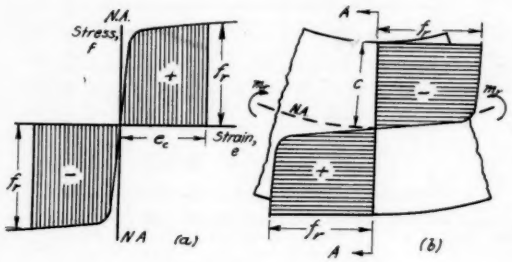

FIG. 2. Rectangular stress distribution.

Trapezoidal Stress Distribution

Consider the condition where the extreme fiber stress f_m of a section subjected to bending lies between the allowable yield stress F_{ty} and the allowable ultimate stress F_{tu}, as shown in Fig. 3(a). The stress-strain distribution has been approximated by a trapezoidal distribution as indicated by the shaded area. The stress indicated by the intercept of the trapezoid with the vertical axis through the origin is designated as the trapezoidal intercept stress f_0. The equivalent trapezoidal distribution is shown on section A-A of Fig. 3(b).

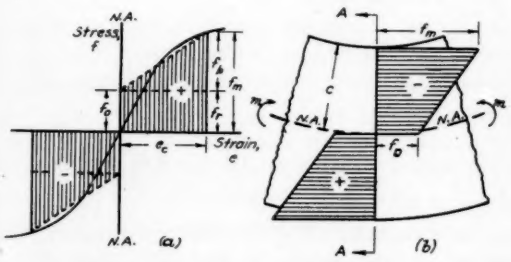

FIG. 3. Trapezoidal stress distribution.

The moment of resistance m of the section subjected to bending may be expressed as

$$m = m_b + m_r \tag{4}$$

since the trapezoidal distribution may be considered as made up of a rectangular distribution with a maximum fiber stress of f_r and a triangular distribution with a maximum fiber stress of f_b.

The values of m_b and m_r when substituted in Eq. (4) will give

$$m = f_b(I/c) + 2f_rQ_m \tag{5}$$

However, it may be seen from Fig. 3(a) that $f_r = f_0$ the trapezoidal intercept stress and that $f_b = f_m - f_0$.

Therefore, these values when substituted in Eq. (5) will give

$$m = (f_m - f_0)(I/c) + 2f_0Q_m \tag{6}$$

By regrouping the terms, this expression may be further reduced to

$$m = f_m(I/c) + f_0[2Q_m - (I/c)] \tag{7}$$

In order to utilize the conventional expression mc/I, divide through by I/c to obtain

$$\frac{mc}{I} = f_m + f_0\left(\frac{2Q_m}{I/c} - 1\right) \tag{8}$$

The term mc/I may be thought of as a measure of the moment of resistance that could be developed by the section, for when multiplied by the section modulus I/c it will give the moment of resistance.

The term $2Q_m/(I/c)$ which depends only on the shape of the cross section is designated by k and will be referred to as the "section factor."

In its final form the expression reduces to

$$mc/I = f_m + f_0(k - 1) \tag{9}$$

Basic Assumptions

In order to apply the expression for trapezoidal distribution to the general problem of plastic bending, the following assumptions are made:

(1) The tensile and compressive stress-strain properties of the material are identical. This gives a simple distribution and avoids the difficulty of a complex distribution. These difficulties will be discussed in the latter part of this article.

(2) The trapezoidal intercept stress f_0 is to be determined so that the first moments about the neutral axis of the area under the actual stress distribution curve are equal to the first moments about the neutral axis of the area under the equivalent trapezoidal stress distribution curve. It is true that such an approximation is exact for a rectangular cross section only.

The variety of cross sections encountered in practice precluded an investigation on all of them. Therefore, it was decided to consider that most aircraft sections could be broken down into three types.

Type (a) is the rectangular type, in which the material is distributed uniformly from the neutral axis to the extreme fiber.

Type (b) is the diamond type in which the amount of material decreases from a maximum at the neutral axis to a minimum at the extreme fiber. Under this

classification would come the solid round and relatively thick-walled tubes.

Type (c) is the more common hour-glass type, in which the amount of material increases from a minimum at the neutral axis to a maximum at the extreme fiber. Under this classification would come the *I*, channel, and most of the tubular sections.

The relative values of trapezoidal stress intercept for these three types have been shown, in the Appendix, to be approximately equal. This implies that the resisting moments for all three types can be predicted by the use of the equivalent trapezoidal distribution based on a rectangular cross section.

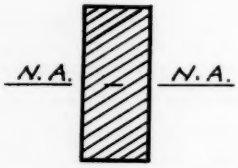

FIG. 4. Type (a). Rectangular type.

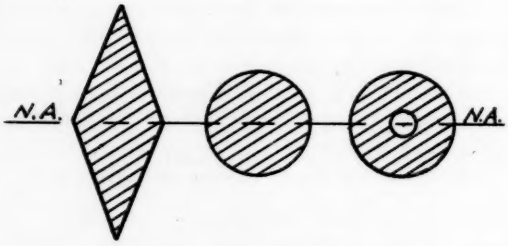

FIG. 5. Type (b). Diamond type.

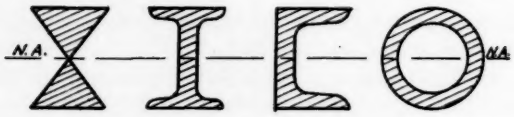

FIG. 6. Type (c). Hour-glass type.

Limits of Factors

The range of values for the section factor k for various sections is shown in Table 1.

It may be interesting to note that Table 1 will be found useful to check preliminary section properties. If the value for a section factor lies outside of the range shown in Table 1, it is fairly certain that an error has been made. This simple check has been used extensively in the Lockheed Engineering Department.

SHEAR DISTRIBUTION

The shear stress distribution corresponding to the trapezoidal bending stress distribution will show a marked change over that obtained from the conventional formula:

$$f_s = SQ/bI \tag{10}$$

TABLE 1
Values of Section Factor, $k = 2Q_m/(I/c)$

Section	Value of k
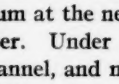	1.0
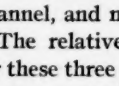	1.5
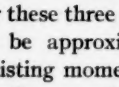	1.0 to 1.5
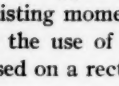	1.0 to 1.5
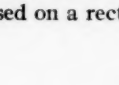	1.25 to 1.70
	2.0
	1.5 to 2.0*
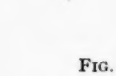	4/3

* Any section having a k value larger than 2.0 should be used with caution as it indicates a relatively thin outstanding leg.

Since it is more convenient to work with shear *flow*, Eq. (10) will be replaced by the equation

$$q = SQ/I \tag{10a}$$

where q equals the shear load per inch.

The new expression for q is derived in the Appendix and may be written as

$$q = \frac{SQ}{I}\left\{\frac{1 + R[(Ac/Q) - 1]}{1 + R(k - 1)}\right\} \tag{11}$$

where Q equals the first moment about the neutral axis, of the area A between the fiber in question and the extreme fiber and R equals df_0/af_m or the rate of change of the trapezoidal intercept stress with respect to the maximum stress.

In the elastic range where the trapezoidal distribution becomes triangular ($f_0 = 0$), the value of R is zero and the expression for shear flow reduces to the conventional form.

DEVELOPMENT OF CURVES OF PLASTIC BENDING AND SHEAR

In order to make use of the relations discussed in the previous pages, certain factors and properties of individual materials will have to be made available.

The basic need is for a complete stress-strain diagram for each material. By complete is meant a diagram that shows the stress-strain properties up to and including the ultimate stress. As the aeronautical structural engineer is faced with more and more refinement of design, the need for complete stress-strain diagrams becomes more urgent. In fact, much of the

future development in structural analysis will be dependent on the plastic stress-strain characteristics of materials.

Stress-strain curves have been assumed for some common aircraft materials so as to satisfy the minimum guaranteed values of: (1) modulus of elasticity, (2) proportional limit, (3) yield stress, (4) ultimate stress, and (5) ultimate elongation.

By means of a tabular form, a copy of which is shown in the Appendix, the stress-strain curve for each of several materials was integrated numerically to give an equivalent trapezoidal distribution with a minimum stress at the neutral axis designated as f_0 and a maximum stress at the extreme fiber designated as f_m. Values of f_m were assumed at various points on the stress-strain curve, and the corresponding f_0 was found so that the first moments about the vertical axis through the origin were equal for (1) the area under the trapezoid and (2) the area under the stress-strain curve. This value of f_0 was substituted into the expression:

$$mc/I = f_m + f_0(k - 1) \qquad (12)$$

for values of $k = 1.0, 1.2, 1.4, 1.6, 1.8$ and 2.0.

The values of intercept stress f_0 were plotted versus f_m and the slope of this curve (df_0/df_m) was in turn computed numerically to give values of R.

Then for each material, there appears on one sheet: (1) a plot of stress f versus strain e, (2) a plot of stress f versus mc/I for various values of k, (3) a plot of stress f versus R, and (4) values of f_0/F_{ty} and f_0/F_{tu}.

All the available curves of this type have been included as Figs. 9 through 17 of this article in the form in which they were used in the Lockheed Engineering Department.

General Discussion of Curves

Bending Stress Distributions

If the complete stress-strain curve of a material were available, any value of extreme fiber stress (f_m) within the limits of the material could be assumed and a complete picture of the actual bending stress distribution over the remainder of the cross section could be had. On the assumption that plane cross sections remain plane after bending, the stress at any intermediate point (y) corresponding to the proportionate strain (e_y) of that point relative to the maximum strain (e_m) of the extreme fiber (i.e., $e_y = (y/c)e_m$) could be determined.

Moments of Resistance Corresponding to an Extreme Fiber Stress (f_m)

Corresponding to any extreme fiber stress (f_m) the moment of resistance m may be found by entering the stress-(mc/I) curve with f_m and determining the mc/I value for the proper "section factor" k.

Then $m = (mc/I)(I/c)$.

Table 2[3]
Comparison of Test and Predicted Moments

1	2	4	16	17
Section	Material	Specimen No.	Ratio Actual To Predicted Moment (15)/(10)	Average X-Ray Rating for Casting
I-Sections	14ST Forging	31	1.104	-
		80	1.105	-
		33	1.079	-
		13	1.064	-
		14	1.070	-
		35	1.045	-
		37	1.039	-
		1	1.054	-
		2	1.028	-
		3	1.020	-
		4	1.059	-
		5	1.030	-
		6	1.040	-
	Mg. Forging	7	1.013	-
		8	1.040	-
		9	1.057	-
		10	1.062	-
		11	1.050	-
		12	1.013	-
	195-T6 Casting	48	1.114	Fair-
		49	1.135	Poor
		75	1.225	-
		78	1.113	-
Round Sections	14ST Forging	15	1.123	-
		79	1.063	-
		17	1.125	-
		19	1.002	-
	195-T6 Casting	39	1.336	Fair
		40	1.131	Fair-
		41	1.440	Fair
Channel Sections	14ST Forging	29	1.078	-
		27	1.037	-
		21	0.965	-
		25	1.095	-
		23	1.024	-
	195-T6 Casting	62	1.054	Poor-
		60	1.080	Poor+
		61	1.235	Fair-
		59	1.075	Poor+
		63-A	1.117	Poor

When the extreme fiber stress is chosen as the allowable yield stress F_{ty}, then the resisting moment will be the allowable yield moment, M_y.

When the extreme fiber stress is chosen as the allowable ultimate stress F_{tu}, then the resisting moment will be the allowable ultimate moment, M_u.

For any applied moment m the corresponding extreme fiber stress and the stress distribution over the entire cross section may be found by entering the curve with mc/I and determining the extreme fiber stress f_m for the proper k value of the section. After the extreme fiber stress has been obtained, the stress distribution over the remainder of the section may be found for any intermediate point as described under the heading "Bending Stress Distributions."

Comparison of Test Results

Simple bending tests[3] had been run at Lockheed on various I, channel, and round sections for 14ST forging, magnesium forging, and 195-T6 castings. Ratios of actual test values to values computed by the proposed method are given in Table 2. A more complete table, showing the computations, is included in the Appendix.

To reduce test results from actual physical properties to minimum guaranteed properties, a correction factor based on the relative first moments of the respective trapezoidal distributions, about the neutral axis, had to be determined. The derivation of this correction factor is also included in the Appendix.

Correction factors were applied to all but the casting tests, since, in the case of casting design, additional factors of safety are included to take care of possible defects in castings. Physical properties of castings determined from a test billet do not necessarily predict the physical properties of the casting proper; therefore, average X-ray ratings for the castings are given in Column 17, Table 2.

Column 16, Table 2, shows the ratio of actual allowable test moments (reduced to minimum guaranteed values except for the castings) to allowable computed moments based on minimum guaranteed properties. There is only one case in which this ratio is less than unity. Specimen 21, which is a channel section of 14ST forged material, shows a ratio of 0.965, which is equivalent to a negative margin of 3.5 per cent. Other specimens from the same billet show positive margins.

The average ratio for the various type sections and materials is given in Table 3.

Margins of Safety

In the plastic range, the margins of safety may no longer be found from the ratio of the allowable stress to the actual stress, since actual stress is no longer directly proportional to loading. The margin of safety must of necessity be found from the ratio of allowable moment to actual moment.

TABLE 3

Section	Material	Average Ratio
I	14ST forging	1.057
	Mg. forging	1.039
	195-T6 casting	1.147
Round	14ST forging	1.078
	195-T6 casting	1.302
Channel	14ST forging	1.040
	195-T6 casting	1.112

Shear Flow

The shear flow (q) for any section may be found by entering the curve with the mc/I value and determining the corresponding value of R for the proper k value of the section. This value of R when substituted in the expression for shear flow will give the desired result.

Shift in Neutral Axis

The actual neutral axis of the section will not always pass through the geometric centroid of the section. For instance, consider the case in which, although the tensile and compressive properties of the material are identical, the section is not symmetric about its centroidal axis. For such a case the neutral axis will no longer coincide with the centroidal axis in the plastic bending range. Although this effect is usually negligible, the designer should be aware of its presence.

Local Crippling

A discussion of modulus of rupture effects would not be complete without mention of local crippling phenomena. This is especially true in connection with structural aircraft practice, since the "Bending Modulus of Rupture Curves for Round Chrome Molybdenum Steel Tubing"[2] has been in use for many years.

An application of the proposed method to "chrome-moly" steel tubes heat-treated to 150,000 lbs. per sq.in., for various ratios of D/T gave results shown by curve AFBC in Fig. 7. Curve DBGE has been reproduced from Figs. 4–20 of ANC-5.[2]

On the surface it would seem that the two methods are inconsistent. The differences, however, in the ranges of D/t larger than 12 may be attributed to the

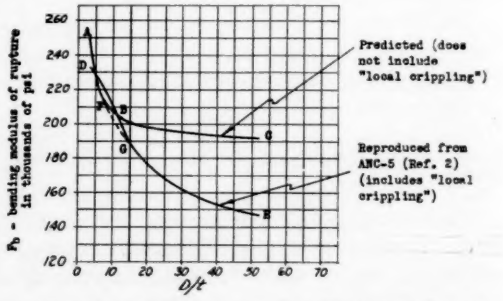

FIG. 7. Bending modulus of rupture "chrome-moly" steel heat-treated to 150,000 lbs. per sq.in.

effects of local crippling. There is a definite need, therefore, for actual crippling data which, if available, could be used as allowable fiber stresses in the proposed method to predict allowable bending moments. For the present it will be conservative to use the proposed method and ensure that no fiber will be stressed beyond its "crippling stress in pure compression," whenever such data are available. For round tubes, however, the ANC-5 bending modulus of rupture curves should be used, since they already include the crippling effects.

Complex Bending

The phenomenon of complex bending, which occurs when the resultant applied moment vector is not parallel to one of the principal axes, is quite common in aircraft practice. The term "complex" bending has been used instead of "unsymmetric" bending, since, even though the word unsymmetric is usually associated with the shape of the section, it is possible for the resultant moment vector to be nonparallel to a principal axis of a simple symmetric shape. The classic beam theory gives a formula for complex bending stress as follows:[5]

$$f_b = \frac{(m_y I_x + m_x I_{xy})x - (m_x I_y + m_y I_{xy})y}{I_x I_y - (I_{xy})^2} \qquad (13)$$

X and Y represent two mutually perpendicular centroidal axes; x and y represent the coordinate distances from the center of gravity measured positive to the right and upward, respectively; m_x equals the applied moment about the X axis, the moment being positive when it tends to put compression in the "upper" fibers; m_y equals the applied moment about the Y axis, the moment being positive when it tends to put compression in the "left" fibers, and I_x, I_y and I_{xy} are the respective moments and product moment of inertia about the X and Y axes.

This formula is applicable only in the elastic range; therefore, it needs to be modified for plastic bending. However, since the development of such a formula is beyond the scope of this article an alternative plan is proposed. In order to clarify the relationship between section properties, applied moments, location of the neutral axis, and principal axes, a review of complex bending in the elastic range will be necessary for complete understanding of the alternative plan.

Consider a rectangular section as shown in Fig. 8. The respective applied moment vectors about the centroidal X and Y axes, which in this case are principal axes, combine to give a resultant moment vector m at an angle of β_r with the X axis. Moment vectors are designated by double-headed arrows. They are to be interpreted by the left-hand rule (i.e., point thumb of left hand as indicated by the double-headed arrow and the natural curl of the remaining fingers of the left hand will designate the direction of moment). This

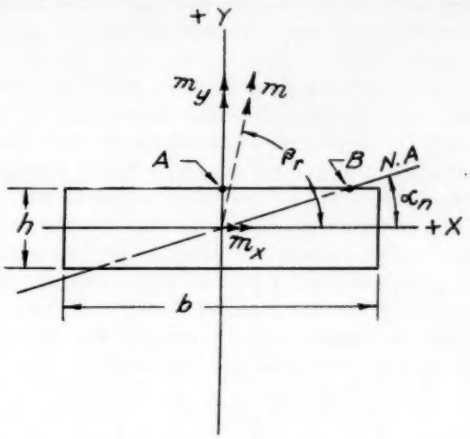

FIG. 8.

implies, therefore, that the moment vector is the axis of the moment.

Let α_n = the angle the neutral axis makes with the X axis in the elastic range

$$= \tan^{-1} \frac{m_y I_x + m_x I_{xy}}{m_x I_y + m_y I_{xy}} \qquad (14)$$

for the general case but, due to the symmetry of this case, it will reduce to:

$$= \tan^{-1} (m_y I_x / m_x I_y) \qquad (15)$$

Let β_r = the angle the resultant applied moment vector makes with the X axis

$$= \tan^{-1}(m_y / m_x) \qquad (16)$$

If the ratio of applied moments m_y/m_x is assumed to be approximately 5 and the ratio of moments of inertia I_x/I_y is assumed to be $^1/_{16}$ when $b/h = 4$, then

$$\alpha_n = \tan^{-1}(5/16) = 17.4°$$
$$\beta_r = \tan^{-1} 5 = 78.7°$$

The section and relative moments shown in Fig. 8 represent the conditions of an actual lug that came up in practice. The large difference in relative position of neutral axis and moment axis as indicated by the angle $\beta_r - \alpha_n$ seems unusual. However, it has purposely been included in this discussion so as to familiarize the structural engineer with this phenomenon. The physical significance of this case indicates that, even though m_x is small relative to m_y, it is still capable of developing a relatively high compressive stress at point A on the section. In fact, the compressive stress in the upper fibers due to m_x is not completely counteracted by the tension stress in the upper right fibers due to m_y until point B is reached.

As long as the maximum stress f_m of the fiber fartherest away from the neutral axis (i.e., the upper left-hand

corner) is below the proportional limit of the material, the neutral axis location will remain as indicated above.

On the other hand, as soon as f_m exceeds the proportional limit and the triangular distribution of stress relative to the neutral axis changes to a trapezoidal distribution, the neutral axis will rotate toward the resultant moment vector. This rotation will be a function of the relative distribution area on either side of the neutral axis as it rotates about the center of gravity of the section. Pending a further study of this phenomenon, it is proposed that the stress-ratio method[6] be applied with a straight-line interaction curve between the following stress ratios:

$$R_x = (m_x/M_x) \text{ and } R_y = (m_y/M_y)$$

where M_x equals the allowable moment about the principal axis X and M_y equals the allowable moment about the principal axis Y.

The margin of safety may then be expressed as

$$\text{M.S.} = [1/(R_x + R_y)] - 1$$

Difference in Compressive and Tensile Properties of a Material

All the preceding derivations and conclusions have been based on the assumption of identical tensile and compressive properties of the material. Although this may not always be true, the means of evaluating a new effective center of gravity of the cross section, based on a different distribution for the tensile and compressive bending stresses, are beyond the scope of this article. Since this situation also occurs in the present usage of the classic beam theory, it is proposed to neglect it, at least until the more important factors are taken care of.

Combined Bending and Direct Load

Many complications enter into a practical means of finding the position of the effective center of gravity. Even the simplest bending case in the plastic range will be subject to this effect when a direct axial load is included. Further study is definitely required with respect to this phenomenon.

Here again it is recommended that the stress-ratio method[6] be used with an interaction between the three stress ratios represented by a plane surface:

$$R_x + R_y + R_a = 1.0$$

where R_x equals m_x/M_x, R_y equals m_y/M_y, and R_a equals f_a/F_a, and where f_a is the applied axial stress, F_a is the allowable axial stress, and x and y subscripts indicate "about the principal X and Y axes," respectively.

The margin of safety in this case may be expressed as

$$\text{M.S.} = [1/(R_x + R_y + R_a)] - 1$$

Summary

The following summary constitutes a presentation of the proposed method suitable for direct engineering use in aircraft work.

General

The conventional beam theory (based on the assumption that a plane section before bending remains plane after bending) gives a linear distribution of strain and stress in the elastic range (i.e., up to the proportional limit). In the plastic range, however, although the strain distribution is assumed to remain linear, the stress distribution corresponds with the stress-strain relationship for the material.

An approximation of this distribution has been obtained which enables the prediction of the effects of shape and material properties on bending in the plastic range.

Graphs are included (Figs. 9 through 17), each of which is applicable to a particular material. These graphs are to be used in connection with the following procedures.

Simple Bending

(A) Determine the "section factor" $k = 2Q_m/(I/c)$. (If $k > 2.0$ use $k = 2.0$.) Q_m is the static (first) moment about the neutral axis of the area between the neutral axis and the extreme fiber. I/c is the conventional section modulus.

(B) *Bending stress* at the extreme fiber due to any applied moment, m. (1) Determine mc/I. (2) Enter the graph with mc/I and obtain the maximum stress, f_m, at the extreme fiber for the proper "section factor" k.

(C) *Bending stress* at an intermediate fiber due to any applied moment, m.

(1) Obtain the stress at the extreme fiber from item (B).

(2) Enter the stress-strain curve with this stress and obtain the maximum strain e_m at the extreme fiber.

(3) At the proper proportional strain e_y of the intermediate fiber, which is at a distance y from the neutral axis, read the corresponding stress, where $e_y = (y/c)e_m$.

(D) *Margins of safety* in bending. (The margins must be determined from the bending moments since stress is no longer proportional to moment.)

(1) Enter the graph with the allowable ultimate tensile stress F_{tu} to obtain an mc/I value for the proper "section factor" k.

(2) Multiply this value by I/c to obtain the allowable ultimate moment M_u.

(3) Repeat (1) using the allowable yield stress F_{ty} to obtain the allowable yield moment M_y.

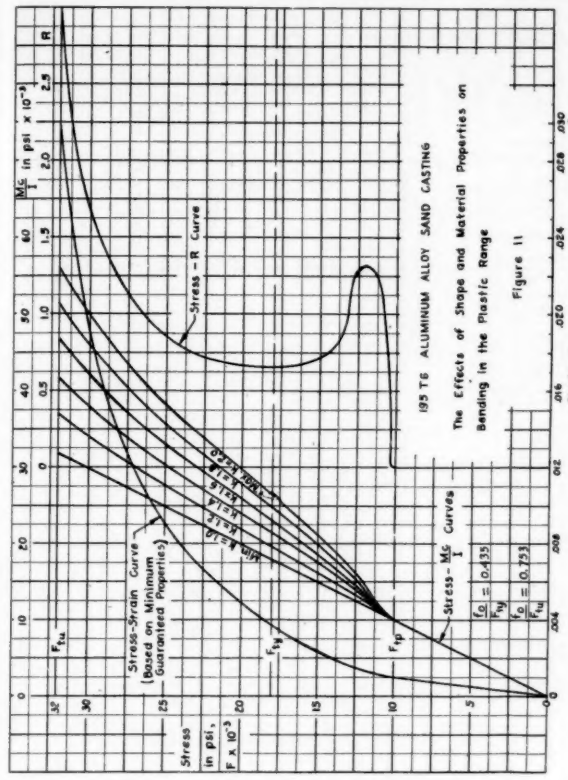
195 T6 ALUMINUM ALLOY SAND CASTING
The Effects of Shape and Material Properties on Bending in the Plastic Range
Figure 11
Stress - R Curve
Stress-Strain Curve (Based on Minimum Guaranteed Properties)
Stress - Mc/I Curves
Stress in psi, F x 10^-3
Strain, e
Based on Minimum Guaranteed Properties

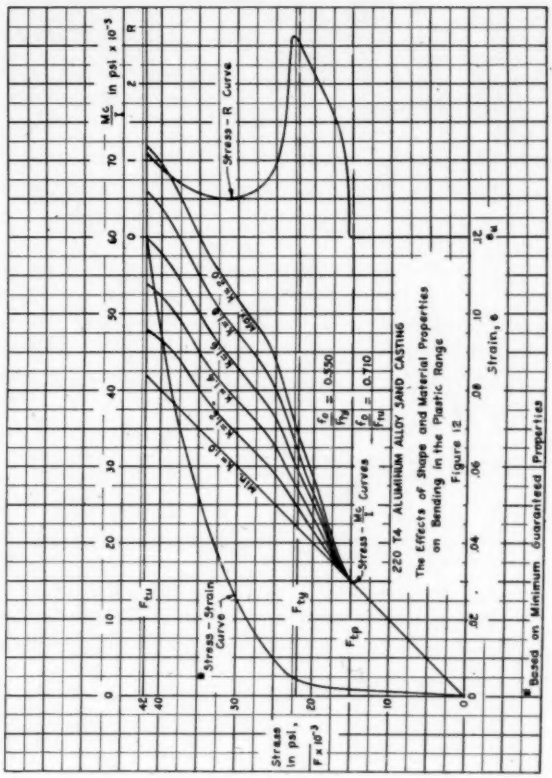
220 T4 ALUMINUM ALLOY SAND CASTING
The Effects of Shape and Material Properties on Bending in the Plastic Range
Figure 12
Stress - R Curve
Stress - Strain Curve
Stress - Mc/I Curves
Stress in psi, F x 10^-3
Strain, e
Based on Minimum Guaranteed Properties

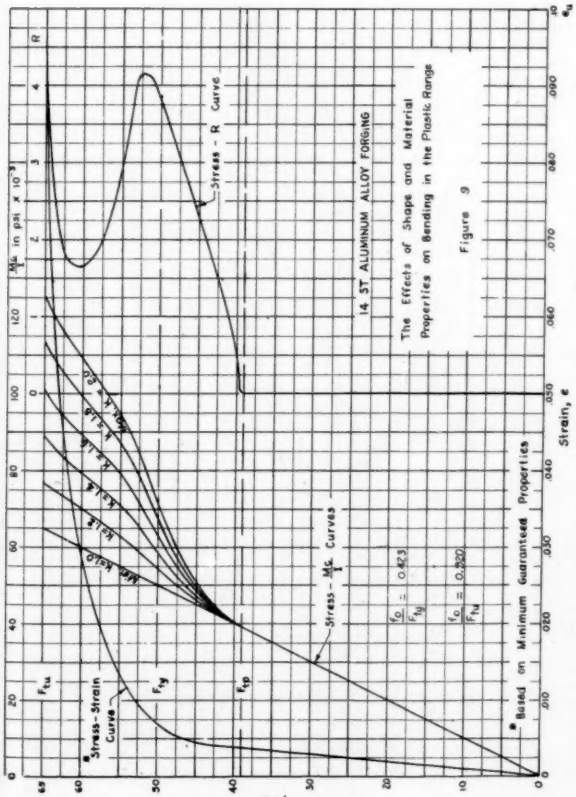
14 ST ALUMINUM ALLOY FORGING
The Effects of Shape and Material Properties on Bending in the Plastic Range
Figure 9
Stress - R Curve
Stress - Strain Curve
Stress - Mc/I Curves
Stress in psi, F x 10^-3
Strain, e
Based on Minimum Guaranteed Properties

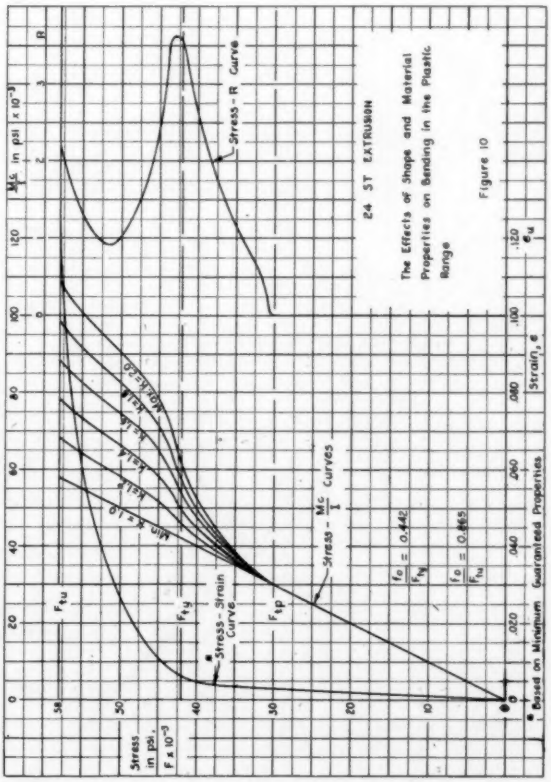
24 ST EXTRUSION
The Effects of Shape and Material Properties on Bending in the Plastic Range
Figure 10
Stress - R Curve
Stress - Strain Curve
Stress - Mc/I Curves
Stress in psi, F x 10^-3
Strain, e
Based on Minimum Guaranteed Properties

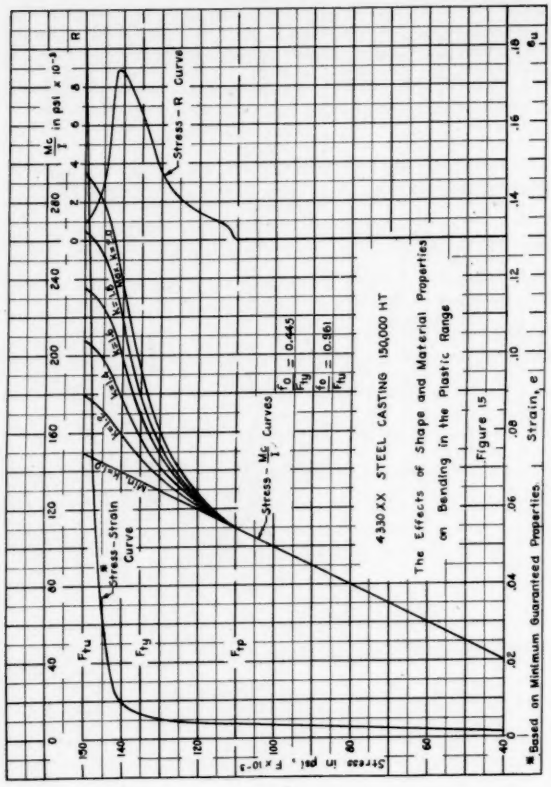
4330 XX STEEL CASTING 150,000 HT
The Effects of Shape and Material Properties on Bending in the Plastic Range
Figure 15
Stress - R Curve
Stress - Strain Curve
Stress - Mc/I Curves
Based on Minimum Guaranteed Properties
Strain, e

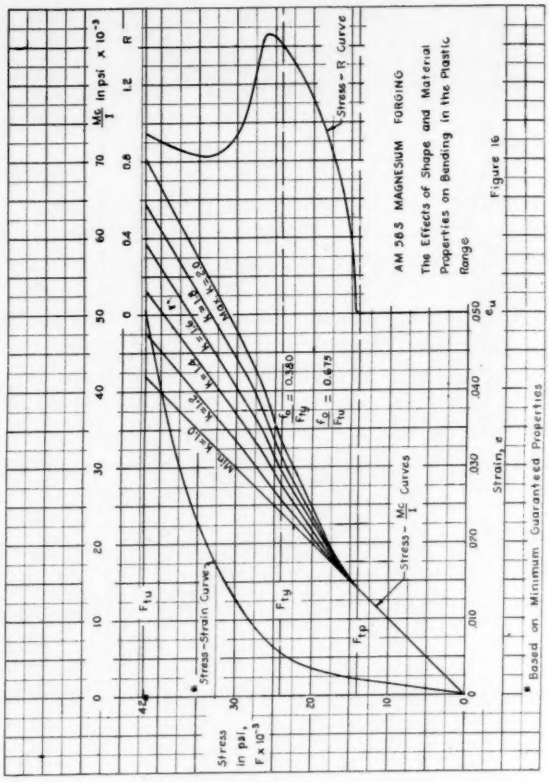
AM 565 MAGNESIUM FORGING
The Effects of Shape and Material Properties on Bending in the Plastic Range
Figure 16
Stress - R Curve
Stress - Strain Curve
Stress - Mc/I Curves
Based on Minimum Guaranteed Properties
Strain, e

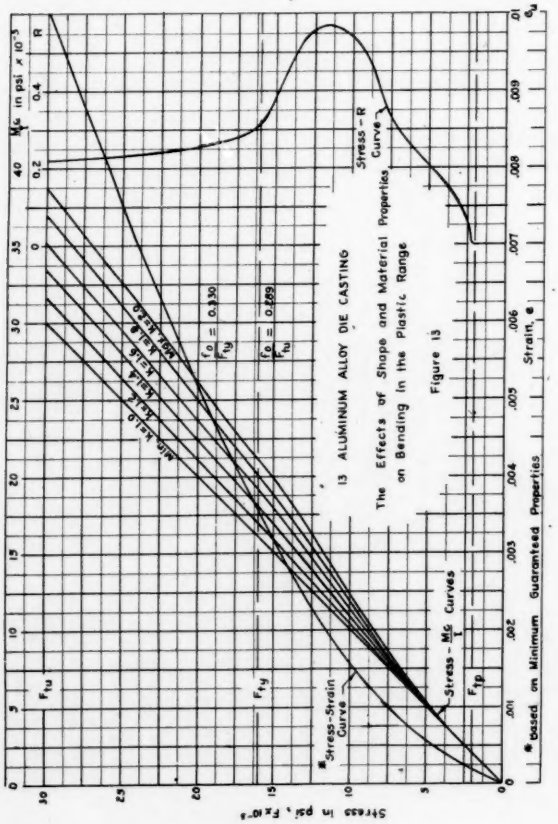
13 ALUMINUM ALLOY DIE CASTING
The Effects of Shape and Material Properties on Bending in the Plastic Range
Figure 13
Stress - R Curve
Stress - Strain Curve
Stress - Mc/I Curves
Based on Minimum Guaranteed Properties
Strain, e

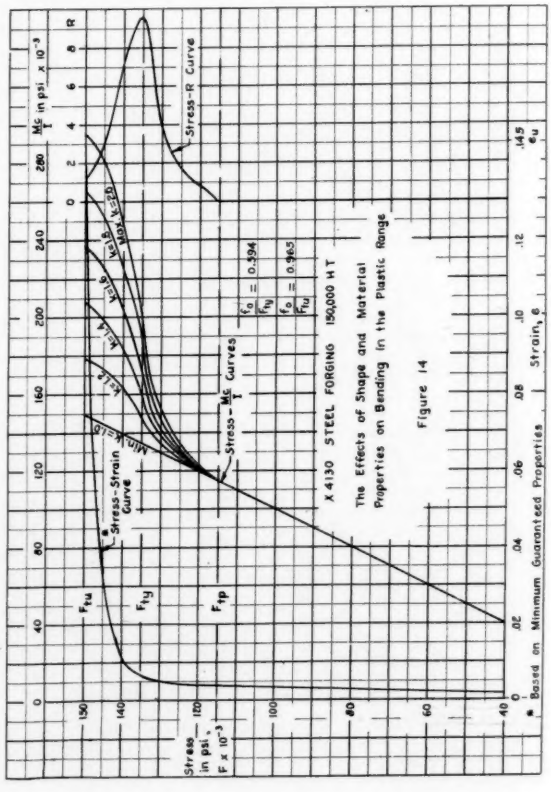
X 4130 STEEL FORGING 150,000 HT
The Effects of Shape and Material Properties on Bending in the Plastic Range
Figure 14
Stress-R Curve
Stress-Strain Curve
Stress - Mc/I Curves
Based on Minimum Guaranteed Properties
Strain, e

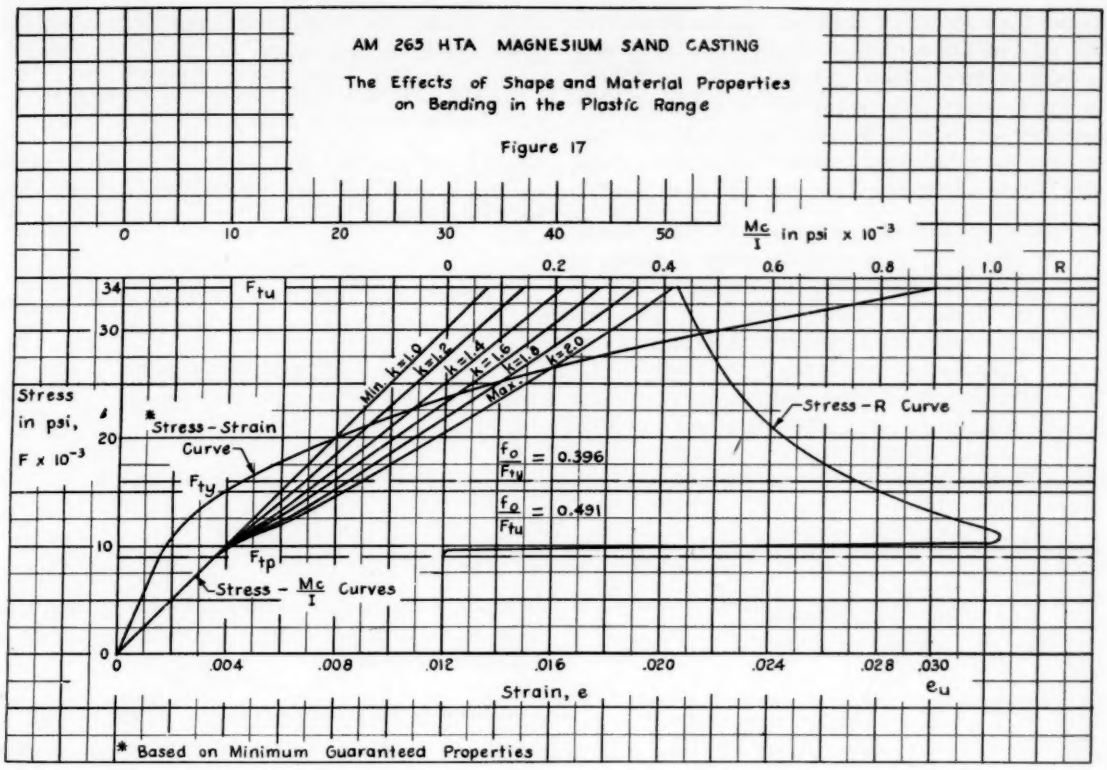

(4) The margin of safety on an ultimate basis:

$$\text{M.S.}_u = (M_u/j_u m_u) - 1$$

j_u is an additional (multiplying) ultimate factor of safety, if any, otherwise use $j_u = 1$. m_u is the applied ultimate moment.

(5) The margin of safety on a yield basis:

$$\text{M.S.}_y = (M_y/j_y m_L) - 1$$

j_y is an additional (multiplying) yield factor of safety, if any, otherwise use $j_y = 1.0$. m_L is the applied limit moment and is usually $= m_u/1.5$.

This method of determining bending allowables has been substantiated by tests on aluminum-alloy castings and forgings, and on magnesium forgings of relatively thick-walled sections only.

(E) *Shear flow* at any fiber due to any applied moment, m, and the corresponding shear, S. The formula that follows is applicable only in the special case where both principal axes are symmetric axes. This method of obtaining shear flow is included in order to indicate how the classic formula SQ/I is modified by the nonlinear stress distribution.

(1) Determine mc/I.

(2) Enter the graph with mc/I and obtain an R value for the proper "section factor" k, where $R = df_0/df_m$, the rate of change of intercept stress f_0 with respect to the maximum stress f_m.

(3) Substitute in the following:

$$q \text{ (shear flow)} = \frac{SQ}{I}\left[\frac{1 + R\left(\frac{Ac}{Q} - 1\right)}{1 + R(k - 1)}\right]$$

where S equals shear load and Q equals static (first) moment about the neutral axis of the area A between the fiber in question and the extreme fiber.

Local Crippling

(A) Assume critical portion of section is developing its crippling stress.

(B) Enter stress-strain curve with this crippling stress and determine the strain of the critical portion, e_y.

(C) Determine the proportionate strain of the extreme fiber e_m, where $e_m = (c/y)e_y$.

(D) Enter the graph with this strain e_m to obtain an mc/I value for the proper "section factor" k.

(E) Multiply this value by I/c to obtain the allowable moment, M, which will subject the critical fiber to its crippling stress.

For round tubes use the bending modulus of rupture curves available in ANC-5 since they include local crippling effects.

Complex Bending

This condition occurs when the resultant applied moment vector is not parallel to a principal axis.

Let X and Y represent two mutually perpendicular centroidal axes; let x and y represent the coordinate

distances from the center of gravity, measured positive to the right and upward, respectively; and let X' and Y' represent the principal axes.

Moment vectors are designated by double-headed arrows and are to be interpreted by the left-hand rule (i.e., point left thumb in direction of vector and natural curl of fingers will designate the direction of moment).

m_x = the applied moment about the X axis, the moment being positive when it tends to put compression in the "upper" fibers

m_y = the applied moment about the Y axis, the moment being positive when it tends to put compression in the "left" fibers

φ = the angle the X' principal axis makes with the original X axis, the angle being positive when measured in a counterclockwise direction.

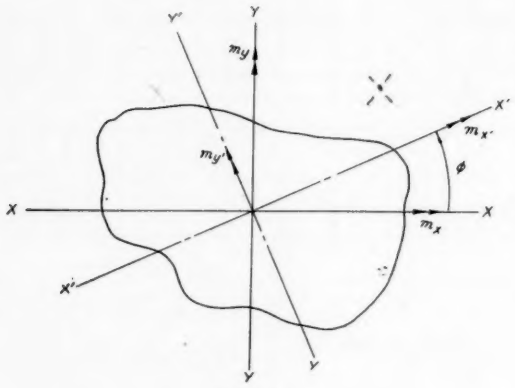

FIG. 18.

Any case of complex bending may be resolved into two cases of simple bending about the principal axes of the section. The principal axes are defined as mutually perpendicular centroidal axes about which the moments of inertia are a maximum and minimum, respectively, and about which the product moment of inertia is zero.

$$I_{\substack{max.\\min.}} = \frac{I_y + I_x}{2} \pm \frac{I_y - I_x}{2} \sec 2\varphi$$

where $\tan 2\varphi = 2I_{xy}/(I_y - I_x)$.

(A) Determine allowable moment $M_{x'}$ as described under simple bending.

$$Q_{mx'} = 0.425\sqrt{I_{x'}A_t} \text{ (approximate formula)}$$

where A_t = total area.

$$c_{x'} = -x \sin \varphi + y \cos \varphi$$

where x and y are the coordinates relative to the original X and Y axes of the fiber fartherest away from the principal X' axis.

$$k_{x'} = 2Q_{mx'}/(I_{x'}/c_{x'})$$

(B) Determine allowable moment $M_{y'}$ as described under simple bending, where

$$Q_{my'} = 0.425\sqrt{I_{y'}A_t} \text{ (approximate formula)}$$
$$c_{y'} = x \cos \varphi + y \sin \varphi$$

where x and y in this case are the coordinates relative to the original X and Y axes of the fiber fartherest away from the principal Y' axis.

$$k_{y'} = 2Q_{my'}/(I_{y'}/c_{y'})$$

(C) Determine applied moments about the principal axes.

$$m_{x'} = m_x \cos \varphi + m_y \sin \varphi$$
$$m_{y'} = -m_x \sin \varphi + m_y \cos \varphi$$

(D) Determine stress ratios.

$$R_{x'} = m_{x'}/M_{x'} \text{ and } R_{y'} = m_{y'}/M_{y'}$$

(E) Determine margin of safety.

$$\text{M.S.} = \{1/[j(R_{x'} + R_{y'})]\} - 1$$

where j is the proper additional factor of safety depending on whether a limit or ultimate margin of safety is involved.

Combined Bending and Axial Load

(A) In a manner similar to that described under "Complex Bending" determine the stress ratios.

$$R_{x'} = m_{x'}/M_{x'} \text{ and } R_{y'} = m_{y'}/M_{y'}$$

(B) Determine $R_a = f_a/F_a$, where f_a is the applied direct stress and F_a is the allowable direct stress.

(C) Determine margin of safety.

$$\text{M.S.} = \{1/[j(R_{x'} + R_{y'} + R_a)]\} - 1$$

where j is the proper additional factor of safety depending on whether a limit or ultimate margin of safety is involved.

(D) Secondary bending should be included when beam columns are being investigated. In such cases it is necessary to determine only the ultimate margin of safety.

REFERENCES

[1] Timoshenko, S., and MacCullough, G. H., *Elements of Strength of Materials*, p. 226; D. Van Nostrand Company, Inc., New York, 1935.

[2] ANC-5, *Strength of Aircraft Elements*, Figs. 4–20, p. 4-35, October, 1940.

[3] Willett, N. L., and Bonza, L., *The Bending Modulus of Cast and Forged Sections*, Lockheed Report No. 2772.

[4] Beilschmidt, J. L., *The Stresses Developed in Sections Subjected to Bending Moment*, Journal of Royal Aeronautical Society, Vol. XLVI, No. 379, pp. 161–182, July, 1942.

[5] Niles, A. S., and Newell, J. S., *Airplane Structures*, 2nd Edition, Vol. 1, p. 164; John Wiley & Sons, Inc., New York, 1938.

[6] Shanley, F. R., and Ryder, E. I., *Stress Ratios*, Aviation, Vol. 35, No. 6, June, 1937.

Tabular Form 77

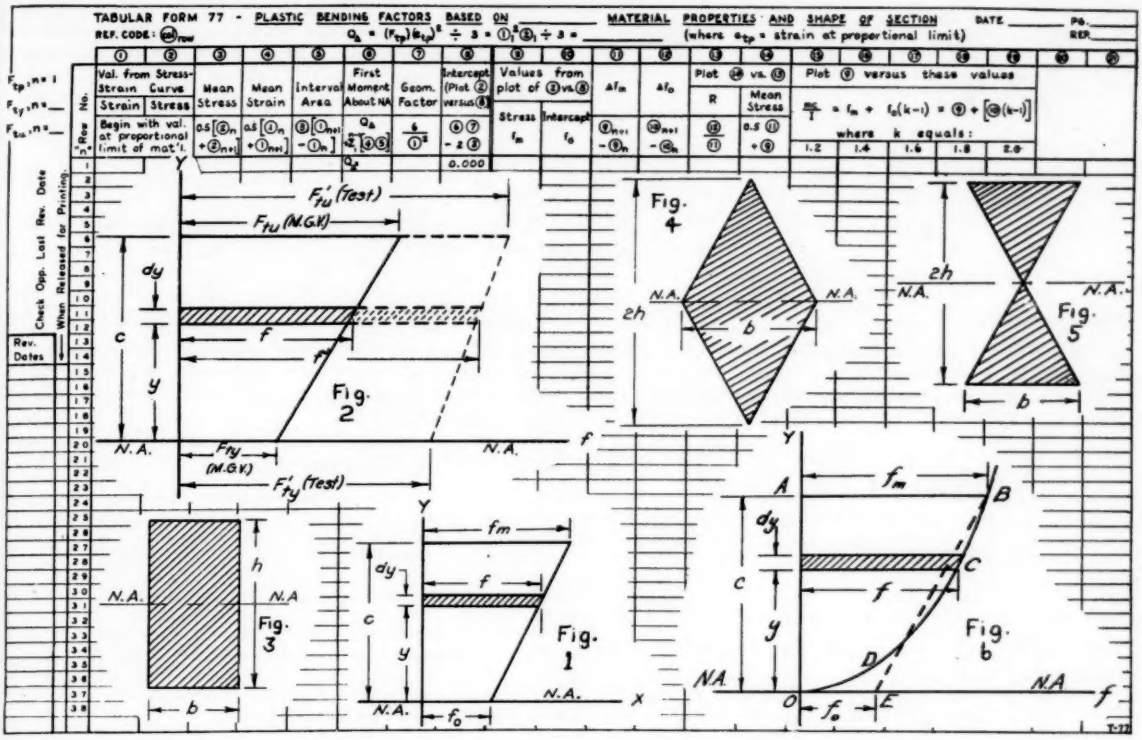

Appendix—Analytic Derivations of Formulas

Moment of Resistance

$$m = 2\int_0^c zfy\,dy$$

where z is width of section at point y (see Fig. 1 superimposed on Tabular Form 77). But

$$f = f_0 + (f_m - f_0)(y/c)$$

$$m = 2\int_0^c \left(f_0 zy + f_m\frac{zy^2}{c} - f_0\frac{zy^2}{c}\right)dy$$

$$= f_m(I/c) + f_0[2Q_m - (I/c)]$$

or

$$mc/I = f_m + f_0(k-1) \qquad (1)$$

where $k = 2Q_m/(I/c)$.

Resisting Load P over a Portion of the Section

P = load on that portion of the cross section between the extreme fiber and the fiber that is at a distance y from the neutral axis

$$P = \int_y^c zf\,dy$$

$$= \int_y^c f_0 z\,dy + (f_m - f_0)\frac{zy\,dy}{c}$$

$$= f_0 A + \frac{(f_m - f_0)}{c}Q = f_m\frac{Q}{c} + f_0\left(A - \frac{Q}{c}\right) \qquad (2)$$

A = area between the extreme fiber and the fiber that is at a distance y from the neutral axis

Q = static (first) moment of area A about the neutral axis

Shear Flow Distribution

$$\frac{mc}{I} = f_m + f_0(k-1)$$

$$\frac{c}{I}\frac{dm}{dx} = \frac{df_m}{dx} + \frac{df_0}{dx}(k-1)$$

$$= \frac{df_m}{dx}\left[1 + \frac{df_0}{df_m}(k-1)\right] = \frac{Sc}{I} \qquad (3)$$

since $S = dm/dx$, from the relation $P = f_m(Q/c) + f_0[A - (Q/c)]$:

$$\frac{dP}{dx} = \frac{df_m}{dx}\frac{Q}{c} + \frac{df_0}{df_m}\frac{df_m}{dx}\left(A - \frac{Q}{c}\right) = q \text{ (shear flow)}$$

Let R = rate of change of trapezoidal intercept stress f_0 with respect to maximum stress = df_0/df_m.

Therefore,

$$q = \frac{df_m}{dx}\left[\frac{Q}{c} + R\left(A - \frac{Q}{c}\right)\right] \qquad (4)$$

But from Eq. (3):

$$df_m/dx = (Sc/I)/[1 + R(k-1)]$$

Substitute in Eq. (4):

$$q = \frac{(Sc/I)\{(Q/c) + R[A - (Q/c)]\}}{1 + R(k-1)}$$

Factor out Q/c

$$q = \frac{SQ}{I}\left\{\frac{1 + R[(Ac/Q) - 1]}{1 + R(k-1)}\right\} \qquad (5)$$

Correction Factor to Reduce Test Data to Minimum Guaranteed Values

In Fig. 2 (superimposed on Tabular Form 77):

$$f = F_{ty} + [(F_{tu} - F_{ty})/c]y$$
$$f' = F_{ty}' + [(F_{tu}' - F_{ty}')/c]y$$

$$\text{Correction factor} = \frac{\int_0^c yf\,dy}{\int_0^c yf'\,dy} = \frac{\int_0^c y\left[F_{ty} + y\frac{F_{tu} - F_{ty}}{c}\right]dy}{\int_0^c y\left[F_{ty}' + y\frac{F_{tu}' - F_{ty}'}{c}\right]dy}$$

$$= \frac{F_{ty}\frac{c^2}{2} + (F_{tu} - F_{ty})\frac{c^2}{3}}{F_{ty}'\frac{c^2}{2} + (F_{tu}' - F_{ty}')\frac{c^2}{3}}$$

$$= (F_{ty} + 2F_{tu})/(F_{ty}' + 2F_{tu}') \qquad (6)$$

Approximation to Q_m

Let $2Q_m = K\rho A_t$. K is a relationship factor, ρ is radius of gyration, and A_t is total area.

Type (a) rectangular cross section (Fig. 3 superimposed on Tabular Form 77):

$$\rho = \sqrt{\frac{I}{A_t}} = \sqrt{\frac{(bh^3/12)}{bh}} = \frac{h}{3.46}$$
$$\rho A_t = bh^2/3.46$$
$$2Q_m = (2bh/2)(h/4) = bh^2/4$$

Therefore,

$$K = 2Q_m/A_t = 0.865$$

Type (b) diamond cross section (Fig. 4 superimposed on Tabular Form 77):

$$\rho = \sqrt{\frac{(2bh^3/12)}{(2bh/2)}} = h/2.45$$
$$\rho A_t = bh^2/2.45$$
$$2Q_m = (2bh/2)(h/3) = bh^2/3$$
$$K = \frac{(bh^2/3)}{(bh^2/2.45)} = 0.817$$

Type (c) hour-glass cross section (Fig. 5 superimposed on Tabular Form 77):

$$\rho = \sqrt{\frac{(2bh^3/4)}{(2bh/2)}} = \sqrt{h^2/2} = h/1.414$$
$$\rho A_t = bh^2/1.414$$
$$2Q_m = (2bh/2)(2h/3) = bh^2/1.5$$
$$K = \frac{(bh^2/1.5)}{(bh^2/1.414)} = 0.943$$

A general value of $K = 0.85$ has been assumed, which in most cases is conservative.

Relative Values of Trapezoidal Stress Intercepts

In Fig. 6 (superimposed on Tabular Form 77):

Let Q_s designate the actual static moment about the N.A. of the area OABCD.

The equivalent trapezoid OABE has a trapezoidal stress intercept $QE = f_0$ and a maximum stress $AB = f_m$ at the extreme fiber.

The equivalence of the trapezoid lies in the fact that f_0 has been determined so that the static moment of the trapezoidal area about the neutral axis is equivalent to Q_s.

This may be written as

$$Q_s = f_0\,c^2/2 + (f_m - f_0)\,c^2/3 \qquad (7)$$
$$= (f_0c^2/6) + (f_mc^2/3)$$

from which

$$f_0 = (6Q_s/c^2) - 2f_m \qquad (8)$$

(Column 8 on Tabular Form 77)

The general expression for equivalent first moments about the neutral axis for a stress-strain distribution and a trapezoidal distribution should include the variation of the cross-sectional width z from the neutral axis to the extreme fiber. This may be written as

$$m = 2\int_0^c yzf\,dy \qquad (9)$$

When z is a constant as in the rectangular type of cross section, the above reduces to

$$m = 2z\int_0^c yf\,dy = 2zQ_s \qquad (10)$$

which indicates that the resisting moment m is directly proportional to the stress-strain static moment Q_s and, therefore, to its equivalent trapezoid as represented by OABE in Fig. 6 superimposed on Tabular Form 77.

However, in the case of the diamond-type cross section where b is the width at the neutral axis:

$$z = b - y(b/c) \qquad (11)$$

$$m = 2\int_0^c yzf\,dy = 2\int_0^c y[f - y(b/c)]f\,dy$$
$$= 2bQ_s - (b/c)I_s \qquad (12)$$

since I_s, the moment of inertia about the neutral axis for area OABCD and a symmetric area below the axis, is

$$I_s = 2\int_0^c y^2f\,dy \qquad (13)$$

This expression for moment may be written in terms of a true equivalent trapezoidal stress intercept designated as f_{0d} and the maximum fiber stress f_m:

$$m = \frac{I}{c}[f_m + f_{0d}(k - 1)] \text{ (see Eq. 9)}$$

Since $k = 2$ for a diamond section (see Table 1):

$$m = (I/c)[f_m + f_{0d}] \qquad (14)$$

Substitute I/c for a diamond section $= bc^2/6$ and equate to Eq. (12):

$$m = \frac{bc^2}{6}(f_m + f_{0d}) = 2bQ_s - \frac{b}{c}I_s \qquad (15)$$

$$f_{0d} = \frac{12Q_s}{c^2} - \frac{6I_s}{c^2} - f_m \qquad (16)$$

But $Q_s = f_0(c^2/6) + f_m(c^2/3)$ (exact value) and $I_s = (f_0c^3/6) + (f_mc^3/2)$ (approximate value). Therefore,

$$f_{0d} = \frac{12}{c^2}\left(f_0\frac{c^2}{6} + f_m\frac{c^2}{3}\right) - \frac{6}{c^2}\left(f_0\frac{c^3}{6} + f_m\frac{c^3}{2}\right) - f_m$$
$$= f_0 \text{ (approximately within 2 per cent)} \qquad (17)$$

In the case of an hour-glass section where b is the width at the extreme fiber:

$$z = (b/c)y \qquad (18)$$

$$m = 2\int_0^c yzf\,dy = 2\int_0^c y[(b/c)y]f\,dy = (b/c)I_s \qquad (19)$$

This expression for moment may be written in terms of a true equivalent trapezoidal stress intercept designated as f_{0h} and the maximum fiber stress f_m;

$$m = \frac{I}{c}[f_m + f_{0h}(k - 1)] \text{ (see Eq. 9)} \qquad (20)$$

Since $k = {}^4/_3$ for an hour-glass section:

$$m = \frac{I}{c}\left[f_m + \frac{f_{0h}}{3}\right]$$

Substitute I/c for an hour-glass section $= bc^2/2$ and equate to Eq. (19).

$$m = \frac{bc^2}{2}\left(f_m + \frac{f_{0h}}{3}\right) = (b/c)I_s \qquad (21)$$

$$f_{0h} = \frac{6}{c^3} I_s - 3f_m \qquad (22)$$

Substitute $I_s = \frac{f_0 c^3}{6} + \frac{f_m c^3}{2}$ (approximate value).

$$f_{0h} = \frac{6}{c^3}\left[f_0 \frac{c^3}{6} + f_m \frac{c^3}{2}\right] - 3f_m$$

$$= f_0 \text{ (approximately within 2 per cent)} \qquad (23)$$

Since true values of the trapezoidal stress intercepts for the three basic types of sections are within 2 per cent of each other, the resisting moments computed on the basis of the trapezoidal stress intercept f_0 for a rectangular section are considered satisfactory.

TABLE 4
Test Data[3]

1	2	3	4	5	6	7	8	9	10	11	12	13	14	15	16	17
Section	Material	Drawing and Part Number	Specimen No.	Billet No.	Section Properties			$\frac{mc}{I}$ at F_{tu} for Proper k	Predicted Allowable Ultimate Moment M_u	Actual Physical Properties From Test		Correction Factor	Actual Moment from Test	Actual Moment Corrected to M.G.V.	Ratio Actual To Predicted Moment	Average X-Ray Rating for Casting
					$\frac{I}{c}$	$2Q_{max}$	k $\frac{(7)}{(6)}$		(6)(9)	F'_{tu}	F'_{ty}	$\frac{2F_{tu}+F_{ty}}{2F'_{tu}+F'_{ty}}$		(13)(14)	$\frac{(15)}{(10)}$	
I-SECTIONS	14ST Forging	X-3495-2	31	4	0.1800	0.2816	1.564	95,700	17,200	68,955	60,050	0.910	20,860	18,970	1.104	-
		-2	80	4	0.1800	0.2816	1.564	95,700	17,200	68,955	60,050	0.910	20,900	19,000	1.105	-
		-3	33	4	0.1314	0.1793	1.365	86,600	11,379	68,955	60,050	0.910	13,480	12,250	1.079	-
		-4	13	2	0.1239	0.1642	1.327	84,500	10,470	66,700	56,950	0.945	11,800	11,130	1.064	-
		-4	14	2	0.1239	0.1642	1.327	84,500	10,470	66,700	56,950	0.945	11,840	11,200	1.070	-
		-5	35	3	0.1165	0.1494	1.283	82,000	9,553	68,650	59,450	0.915	10,980	10,000	1.045	-
		-6	37	3	0.0971	0.1296	1.335	85,000	8,254	68,650	59,450	0.915	9,360	8,560	1.039	-
		X-3093-1	1	1	0.1667	0.2500	1.500	95,000	15,800	67,940	59,975	0.920	18,120	16,670	1.054	-
		-1	2	1	0.1667	0.2500	1.500	95,000	15,800	67,940	59,975	0.920	17,680	16,250	1.028	-
		-2	3	1	0.1603	0.2240	1.397	88,800	14,235	67,940	59,975	0.920	15,760	14,500	1.020	-
		-2	4	1	0.1603	0.2240	1.397	88,800	14,235	67,940	59,975	0.920	16,400	15,070	1.059	-
		-3	5	1	0.1260	0.1600	1.270	81,200	10,231	67,940	59,975	0.920	11,440	10,530	1.030	-
		-3	6	1	0.1260	0.1600	1.270	81,200	10,231	67,940	59,975	0.920	11,560	10,630	1.040	-
	Magnesium Forging	-1	7	2	0.1667	0.2500	1.500	56,250	9,377	50,715	35,125	0.792	12,000	9,500	1.013	-
		-1	8	2	0.1667	0.2500	1.500	56,250	9,377	50,715	35,125	0.792	12,320	9,750	1.040	-
		-2	9	1	0.1603	0.2240	1.397	53,100	8,512	50,725	32,790	0.805	11,160	9,000	1.057	-
		-2	10	2	0.1603	0.2240	1.397	53,100	8,512	50,715	35,125	0.792	11,420	9,050	1.062	-
		-3	11	1	0.1260	0.1600	1.270	49,400	6,224	50,725	32,790	0.805	8,120	6,540	1.050	-
		-3	12	1	0.1260	0.1600	1.270	49,400	6,224	50,725	32,790	0.805	7,840	6,310	1.013	-
	195-T6 Casting	-1	48	3	0.1667	0.2500	1.500	44,000	7,335	35,930	27,500	No	8,160	8,160	1.114	Fair-
		-2	49	3	0.1603	0.2240	1.397	41,500	6,652	35,930	27,500	Reduction	7,552	7,552	1.135	Poor
		-3	75	3	0.1260	0.1600	1.270	38,750	4,883	37,060	28,675	Factor	5,976	5,976	1.225	-
		-3	78	3	0.1260	0.1600	1.270	38,750	4,883	37,060	28,675		5,440	5,440	1.113	-
Round Section	14ST Forging	X-3252-1	15	2	0.0982	0.1670	1.700	107,000	10,507	66,700	56,950	0.945	12,480	11,800	1.123	-
		-1	79	4	0.0982	0.1670	1.700	107,000	10,507	68,955	60,050	0.910	12,280	11,170	1.063	-
		-2	17	2	0.0854	0.1310	1.535	97,100	8,292	66,700	56,950	0.945	9,880	9,340	1.125	-
		-3	19	5	0.0580	0.0810	1.396	88,500	5,133	68,975	59,700	0.910	5,660	5,150	1.002	
	195-T6 Casting	-1	39	3	0.0982	0.1670	1.700	49,000	4,812	35,930	27,500	No	6,424	6,424	1.336	Fair
		-2	40	4	0.0854	0.1310	1.535	44,750	3,832	31,935	26,900	Reduction	4,328	4,328	1.131	Fair-
		-3	41	3	0.0580	0.0810	1.396	41,400	2,401	35,930	27,500	Factor	3,456	3,456	1.440	Fair
Channel Section	14ST Forging	X-3496-2	29	2	0.1176	0.1806	1.537	97,200	11,431	66,700	56,950	0.945	13,040	12,320	1.078	-
		-3	27	5	0.0950	0.1378	1.453	92,200	8,759	68,975	59,700	0.910	9,980	9,080	1.037	-
		-4	21	5	0.0884	0.1212	1.372	87,300	7,717	68,975	59,700	0.910	8,200	7,450	0.965	-
		-5	25	5	0.0685	0.1020	1.490	94,400	6,466	68,975	59,700	0.910	7,780	7,080	1.095	-
		-6	23	3	0.0605	0.0836	1.383	88,000	5,324	68,650	59,450	0.915	5,960	5,450	1.024	-
	195-T6 Casting	X-3494-2	62	2	0.1296	0.1838	1.419	42,000	5,443	36,295	28,725		5,740	5,740	1.054	Poor-
		-3	60	2	0.1082	0.1444	1.337	40,400	4,371	36,295	28,725	No	4,720	4,720	1.080	Poor+
		-4	61	2	0.0997	0.1259	1.264	38,600	3,848	36,295	28,725	Reduction	4,752	4,752	1.235	Fair-
		-5	59	2	0.0711	0.0975	1.372	41,000	2,915	36,295	28,725	Factor	3,136	3,136	1.075	Poor+
		-6	63-A	4	0.0660	0.0864	1.310	39,600	2,614	31,935	26,900		2,920	2,920	1.117	Poor

A New Method of Longitudinal Control for Aircraft by Use of an Adjustable Angle of Attack Balance

ROLAND J. WHITE*

Curtiss-Wright Corporation

Introduction

THE PRESENT-DAY TYPE of large airplane has approached a definite limit in two respects: first, it must be loaded over a restricted center of gravity range (c.g. range); second, as the airplane size and gross weight are increased, the control forces become too great unless properly reduced, which so far has been a troublesome problem.

The c.g. range of the airplane has the forward limit fixed by the maximum control force that can be produced by the horizontal tail to meet a given landing or maneuvering requirement and the rearward c.g. limit established by the ability of the airplane to meet certain stability requirements. Lately, these stability requirements have offered much discussion, mainly because airplanes may still be flown at c.g. positions further aft than the position generally limited by the requirements.

In this paper, the author presents a new method of aircraft longitudinal control which it is believed will permit the c.g. range of the airplane to be substantially increased, as well as reduce the control forces in a more satisfactory manner than is customary. This method essentially provides a cockpit control by which the pilot may regulate the elevator hinge moment characteristics according to an estimate of the airplane c.g. and enables the pilot to make the airplane stable during a climb or in level cruising flight or maneuverable when he so desires. The cockpit control is a means for regulating the amount the elevator hinge moment changes for a given change in angle of attack of the airplane horizontal tail as expressed by the elevator hinge moment coefficient derivative $\partial C_{He}/\partial \alpha_t = C_{He\alpha}$.

To obtain this regulation a method is proposed whereby the forward part of the stabilizer is made movable and is connected to the elevator by an adjustable linkage system such that it may move in a regulated manner with the elevator. A second method consists of allowing a small surface within the stabilizer to move in an adjustable relation to a tab attached to the elevator, the internal surface being vented to the airfoil surface.

In the first part of the paper the elevator control forces are analytically calculated in order to show how the various physical characteristics of the airplane effect the longitudinal control forces. Following this, an example airplane having arbitrary dimensions is selected, and control forces are calculated in order to demonstrate the use of the developed equations and to indicate the improvements that may be realized if $C_{He\alpha}$ is properly regulated. In the second part of the paper wind-tunnel results of the two methods of regulating $C_{He\alpha}$ are given along with charts and equations permitting the engineer to design properly such a control system.

It is believed that future airplanes may have their c.g. range extended to twice the present permissible range if proper regulation of the hinge moment derivative $C_{He\alpha}$ is made possible.

Symbols Used

b	= wing span (ft.)
l_h	= distance from c.g. to elevator hinge line (ft.)
MAC	= wing mean aerodynamic chord (ft.)
h	= length of control column (ft.)
ϕ	= angular position of control column
c_θ	= effective moment arm of internal pressure surface (ft.)
c_e, c_δ	= MAC of elevator and tab, respectively (ft.)
D_1, D_2, D_3	= airplane aerodynamic constants defined by Eqs. (6), (10), and (13)
C	= constant involving the mechanical advantage of the elevator control system
R	= ratio of moment transmitted from balance surface to tab or elevator to that developed by the balance surface (positive if moment tends to deflect elevator or tab in a positive direction)
R_w	= wing aspect ratio
R_V, R_n	= aerodynamic constants defined by Eqs. (25) and (28)
N	= speed ratio given in Eq. (21)
σ	= density ratio
V	= air speed (ft. per sec.)
$\bar{V}$	= tail volume = $(S_t/S)(l_h/MAC)$
η_t	= tail efficiency factor = (V at tail/V)^2
q	= angular pitch velocity (rad. per sec.)
n	= airplane load factor
F_V, F_n	= elevator control forces given by Eqs. (23) and (27)
G	= distance from airplane aerodynamic center (a.c.) for tail-off to airplane c.g. in fraction of wing MAC (positive for c.g. forward of a.c.)
l_w	= airplane wing loading (lbs. per sq.ft.)
S, S_t, S_e, S_θ, S_δ	= areas of wing, tail, elevator, internal balance surface, and tab, respectively (sq.ft.)

Presented at the Airplane Design Session, Eleventh Annual Meeting, I.Ae.S., New York, January 25–29, 1943.

* Aerodynamicist, Airplane Division.

C_L = airplane lift coefficient (neglecting tail lift)
C_{L0} = airplane lift coefficient such that C_m tail-off equals C_m tail-on for $e = 0$
C_{Lm} = maximum lift coefficient
C_{Lt} = tail lift coefficient
k_e, k_θ = elevator and external balance effectiveness (taken as positive)
m_w, m_t = $dC_L/d\alpha$ for wing and tail (C_L/deg.)
C_m = airplane pitching moment coefficient
C_{m0} = airplane pitching moment coefficient at $C_L = 0$ for $e = 0$
C_{mt} = airplane pitching moment coefficient due to the horizontal tail
$C_{m\dot{\alpha}t}$, $C_{m\dot{\alpha}}$ = airplane pitching moment coefficient developed due to angular pitch velocity for tail and for airplane minus tail
Cm_q = $\partial Cm/\partial(qb/2V)$ for airplane minus tail
C_{He}, $C_{H\delta}$ = hinge moment coefficient of elevator and tab based on their respective chords and areas (a line over the "C" indicates the elevator or tab acting with balance surface)
C_{HN} = hinge moment coefficient of external balance surface based upon the elevator chord and area
C_{HA} = $\partial C_{HN}/\partial C_{Lt}$ for $e = 0$
$C_{HB\theta}$, C_{HBe} = $\partial C_{HN}/\partial\theta$, $\partial C_{HN}/\partial e$ for $C_{Lt} = 0$
C_{Hee}, $C_{He\alpha}$, etc. = $\partial C_{He}/\partial e$, $\partial C_{He}/\partial\alpha_t$ for α or e constant. The second subscript indicates the variable of the derivative
P = ratio of pressure difference between the upper and lower surfaces of the airfoil at some chordwise position (x/c) divided by $(\rho/2)V^2$

Basic Control Force Equations

In developing the basic control force equations the following assumptions will be made: (1) Airplane pitching moments and their components are linear with C_L; (2) Horizontal tail lift and elevator hinge moments are linear with tail angle of attack and elevator deflection; (3) All accelerations are neglected except the normal acceleration due to a curved flight path.

Assumptions (1) and (2) are convenient but may not be applicable to many present airplanes; however, it is believed that for future large airplanes these conditions must be realized before efficient longitudinal control will be obtained.

Referring to the list of symbols, the airplane pitching moment coefficient in rectlinear flight for the airplane without tail may be written as

$$C_m = C_{m0} - GC_L \tag{1}$$

To this pitching moment coefficient must be added that due to the tail. The tail pitching moment coefficient is influenced by the down-wash from the wing, which may be represented by $d\alpha_t/d\alpha$. From elementary down-wash theory for the tail a normal distance behind the wing,

$$d\alpha_t/d\alpha = [1 - 2(57.3)m_w/\pi R_w] \tag{2}$$

The tail lift coefficient is expressed as

$$C_{Lt} = m_t(\alpha_t + k_e e) \tag{3}$$

and defining the tail volume as

$$\bar{V} = (S_t/S)(l_h/MAC) \tag{4}$$

the tail pitching moment coefficient may be written as

$$C_{mt} = -\eta_t\bar{V}D_1(C_L - C_{L0}) - \eta_t\bar{V}m_t k_e e \tag{5}$$

where

$$D_1 = (m_t/m_w)d\alpha_t/d\alpha \tag{6}$$

Having determined the airplane pitching moment components for rectlinear flight the effects of a curved flight path will be considered. For a pull-up from level flight the airplane lift coefficient is

$$C_L = nl_w/(\rho/2)V^2 \tag{7}$$

and for a given load factor n the angular pitch velocity q, expressed in radians per second, is

$$q = (n - 1)g/V \tag{8}$$

The above relations permit the increment of angle of attack at the tail due to q to be calculated as

$$\Delta\alpha_t = [(n - 1)/n]D_2C_L \tag{9}$$

where

$$D_2 = 2.19l_h\sigma/\sqrt{\eta_t}\,l_w \tag{10}$$

here, $2.19 = 0.002378(32.2)(57.3)/2$. The corresponding damping moment in pitch because of the horizontal tail then becomes

$$C_{m\dot{\alpha}t} = -\eta_t\bar{V}m_tD_2[(n - 1)/n]C_L \tag{11}$$

In addition to this damping moment the wing and fuselage will contribute a damping moment that is about 25 per cent of that of the tail for a normal type airplane.

In the present notation this damping moment coefficient may be expressed as

$$C_{m\dot{\alpha}} = [(n - 1)/n]D_3C_L \tag{12}$$

here

$$D_3 = 0.0191C_{mq}\sigma b/l_w \tag{13}$$

where $0.0191 = 0.002378(32.2)/4$. Now combining the pitching moment increments from Eqs. (1), (5), (11), and (12) the total airplane pitching moment equation becomes,

$$C_m = [C_{m0} + \eta_t\bar{V}D_1C_{L0}] - \left[G + \eta_t\bar{V}D_1 + \left(\frac{n - 1}{n}\right)(\eta_t\bar{V}m_tD_2 - D_3)\right]C_L - \eta_t\bar{V}m_tk_e e \tag{14}$$

In order to find the most forward value of G for trim of the airplane let $C_L = C_{Lm}$, $C_m = 0$, $k_e e = (k_e e)_m$; then

$$G_f = \left[\frac{C_{m0}}{C_{Lm}} - D_3\right] - \eta_t\bar{V}\left[D_1\left(1 - \frac{C_{L0}}{C_{Lm}}\right) + (m_t(k_e e)_m/C_{Lm}) + \frac{(n - 1)}{n}D_2m_t\right] \tag{15}$$

This forward c.g. position represents the limit for control, assuming, of course, that the pilot can exert

enough control force to produce the maximum elevator deflection desired. The next problem is to relate the elevator control force with the airplane pitching moment coefficient. To do this, express the elevator hinge moments by the equation

$$C_{He} = C_{He\alpha}\alpha_t + C_{Hee}e \tag{16}$$

During a maneuver a definite value of e will be required which may be found from Eq. (14) for the condition that $C_m = 0$; also a corresponding angle of attack of the tail will occur which may be determined from Eqs. (3) to (9). It will now be assumed that the airplane is in trim in level flight at a speed V_1 giving C_{L1}, and a maneuver is made to a new value of $C_L = C_{L2}$; then the change in elevator angle necessary to produce this change in C_L as found from Eq. (14) is

$$\Delta e = \frac{-1}{m_t k_e}\left[\frac{G}{\eta_t \bar{V}} + D_1 + m_t D_2 - \frac{D_3}{\eta_t \bar{V}}\right](C_{L2} - C_{L1}) \tag{17}$$

and the corresponding change in tail angle of attack is

$$\Delta\alpha_t = [(D_1/m_t) + D_2](C_{L2} - C_{L1}) \tag{18}$$

From these relations the change in elevator hinge moment coefficient becomes

$$\Delta C_{He\alpha} = C_{He}:\Delta\alpha_t + C_{Hee}\Delta e \tag{19}$$

The elevator control force F will depend upon the mechanical advantage of the control system which is assumed constant for all control positions and indicated by the derivative $d\phi/de$. As the elevator hinge moments are based upon the elevator area and chord, the maximum control force required to maneuver is

$$F = [S_e c_e/h(d\phi/de)][(\rho/2)V^2](\Delta C_{He}) \tag{20}$$

There are two types of manuevers to be considered. The first type assumes that C_{L2} is obtained by allowing the air speed to change to V_2 with no appreciable acceleration. For this case let $n = 1$ and introduce

$$N = V_1/V_2 \tag{21}$$

then

$$C_{L2} - C_{L1} = [l_w/(\rho/2)V_1^2][N^2 - 1] \tag{22}$$

Using the relations of Eqs. (17), (18), (19), (20), and (22) this control force, denoted as F_V, may be expressed as

$$F_V = CR_V[1 - 1/N^2] \tag{23}$$

where

$$C = S_e c_e l_w/h(d\phi/de) \tag{24}$$

$$R_V = \frac{-C_{Hee}}{m_t k_e}\left[D_1\left(1 - k_e\frac{C_{He\alpha}}{C_{Hee}}\right) + \frac{G}{\eta_t \bar{V}}\right] \tag{25}$$

The second type of maneuver is produced by a pull-up or highly banked turn that produces an acceleration but does so without an appreciable change in air speed. For this case the velocity V of Eq. (2) remains constant at $V = V_1$ and

$$C_{L2} - C_{L1} = (n - 1)l_w/(\rho/2)V_1^2 \tag{26}$$

Using this relation in a similar manner, as was done in the first case the control force, denoted as F_n, that is required to perform this maneuver will be independent of the air speed and given by the equation

$$F_n = CR_n(n - 1) \tag{27}$$

where

$$R_n = \frac{-C_{Hee}}{m_t k_e}\left[(D_1 + D_2 m_t)\left(1 - k_e\frac{C_{He\alpha}}{C_{Hee}}\right) + \left(\frac{G - D_3}{\eta_t \bar{V}}\right)\right] \tag{28}$$

Eqs. (23) and (27) represent the basic control force equations and may be used in combination if necessary to calculate any longitudinal control maneuver.

The interpretation of these basic control force equations may best be studied by applying them directly to an airplane. This will be done in the following section.

Calculations and Discussion of Control Forces for a Typical Large Airplane

A typical large airplane of arbitrary dimensions has been chosen and the control forces have been calculated. It will be assumed that the elevator has a high degree of aerodynamic balance ($C_{Hee} = -0.002$) and can maintain this balance at all elevator angles from $e = +10°$ to $e = -25°$. A constant mechanical advantage of the control system will be assumed such as to permit an 18-in. fore-and-aft movement of a 3.0-ft. control column. The horizontal tail is assumed to have a 40 per cent chord elevator that is capable of producing a maximum value of $(k_e e)_m = -10$ which is used in determining the forward c.g. position for trim. This assumes that k_e will reduce in value at a large elevator angle; hence, the control force required to produce $e = 25°$ elevator deflection will be larger than those calculated. This condition would require a special investigation and will not be made here.

Airplane Dimensions

Gross weight = W = 50,000 lbs.
Wing area = S = 1300 sq.ft.
Wing loading = l_w = 38.5 lbs. per sq.ft.
Wing span = b = 102 ft.
Wing MAC = 13.35 ft.
Wing aspect ratio = R = 8.0
Slope of wing lift curve = $m_w = 0.080C_L$/deg.
Distance from c.g. to elevator hinge axis = l_h = 40 ft.
Tail area = S_t = 175 sq.ft.
Tail area ratio = S_t/S = 13.45 per cent
Overall span of tail = 28.0 ft.
Tail aspect ratio = 4.48

Elevator chord = 2.50 ft.
Elevator area = 65 ft.
Slope of tail lift curve = $m_t = 0.050C_L$/deg.
Elevator hinge axis 60 per cent chord position from L.E. of stabilizer
Elevator effectiveness = $k_e = 0.670$
Maximum effective change in tail angle of attack due to deflecting the elevator = $(k_e e)_m = -10°$
Tail efficiency = $(V_t/V)^2 = 0.90$
Effective tail volume = $0.90(0.1345)(40/13.35) = 0.363$

Calculated Constants

$C_{m_0} = -0.006$
$C_{Lm} = 1.5$
$a.c. = 0.15\ MAC$ from L.E. for tail-off
$D_1 = 0.397$ $D_3 = 0.010$ (Estimated)
$D_2 = 2.40$ for $\sigma = 1.0$ $C = 2540$

These dimensions are first used with Eq. (23) to calculate the control force experienced during an unaccelerated pull-up, assuming that the airplane is in trim at a given air speed and that a climb is started such to reduce the air speed by 20 per cent before a change in trim is made. These forces are calculated for various c.g. positions using different values of $C_{H_{e\alpha}}$ and plotted in Fig. 1. From Eq. (15) the most forward c.g. for trim is 15.5 per cent of the wing MAC from its leading edge. It will now be assumed that in obtaining an aerodynamic balance giving $C_{H_{ee}} = -0.002$ a value of $C_{H_{e\alpha}} = -0.0005$ will result for the normal airplane. If, however, $C_{H_{e\alpha}}$ is regulated such that dCm/dC_L for the airplane with elevator free maintains a constant value of static stability—say, -0.05 for the elevator free condition—then the curve labeled 5 per cent static stability in Fig. 1 will result. If $C_{H_{e\alpha}}$ could be controlled to ± 0.0020 for this airplane a c.g. range from 15.5 to 34.5 per cent of the MAC would result while still having 5 per cent static stability. In this case the most rearward c.g. for $dCm/dC_L = 0$ for elevator free would be 39 per cent of the MAC. If $dCm/dC_L = 0$ for elevator free is adopted for the criterion in determining the most rearward c.g. position, the normal airplane would have a 11 per cent c.g. travel, while with proper control of $C_{H_{e\alpha}}$ a c.g. range of 23.5 per cent would result. It is well to note here that had the value of $C_{H_{ee}} = -0.002$ been obtained by using a normal type balancing tab a value of $C_{H_{e\alpha}} = -0.004$ would result which would make the airplane unstable at all c.g. positions.

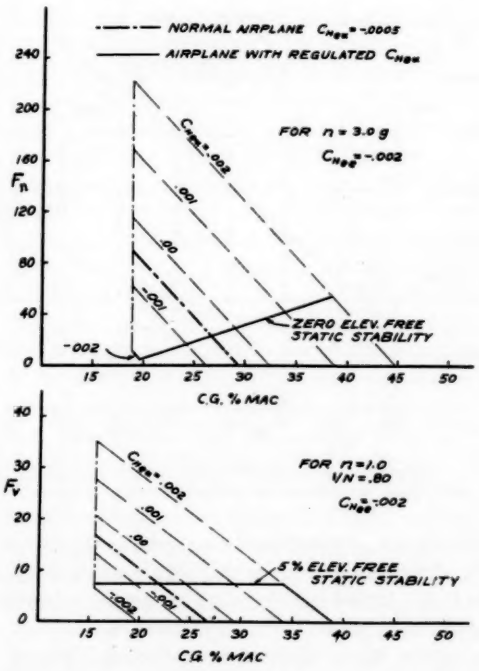

FIG. 1. Calculated control forces for example airplane.

In Fig. 1, curves of the control forces experienced during a $3g$ pull-out at constant air speed are also shown as calculated from Eq. (27). During this type of maneuver the most forward c.g. position is limited to 19 per cent if it is necessary to maneuver at a reduced speed such as to give $C_{Lm} = 1.5$ at a $3g$ maneuver. Now if the most rearward c.g. is selected as in the above paragraph for the unaccelerated flight maneuver, then the normal airplane would have a c.g. range from 19 to 26.5 per cent which would result in a maximum control force of 90 lbs.; while, if $C_{H_{e\alpha}}$ could be controlled such as to maintain zero static stability for elevator free, the airplane would have a c.g. range from 19 to 39 per cent with a maximum control force of 55 lbs. This indicates that by regulating $C_{H_{e\alpha}}$ the c.g. range has been extended 2.67 times while reducing the maximum control forces by 39 per cent. It is felt that if the airplane would have an adjustable angle of attack balance that would double the c.g. range it would be sufficiently satisfactory.

Further interpretation of these figures will not be made, but they show the resulting advantage that may be obtained if proper regulation of $C_{H_{e\alpha}}$ is made during flight. By proper use of the basic control force equations the control forces for any proposed airplane may be calculated and the requirements for the detailed aerodynamic design established.

There are other factors that may limit the c.g. range indicated by the above equations and the extent to which $C_{H_{e\alpha}}$ may be controlled. These factors cannot be discussed here but will be outlined as follows:

(a) Effect of landing with and without flaps.

(b) Effect of k_e being reduced at large elevator angles including trim tab effect.

(c) Effect of dynamic stability of the airplane for the elevator free condition.

(d) Effect of slipstream on the airplane pitching moments.

(e) Effect of compressibility at high speed.

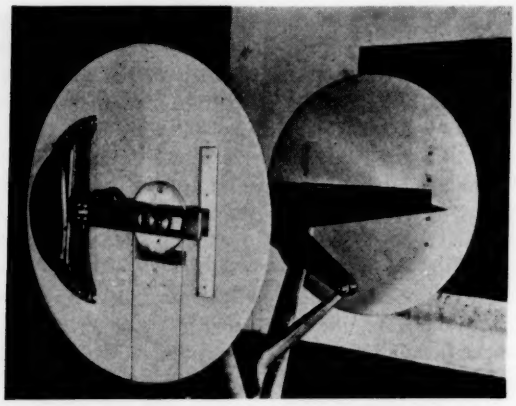

FIG. 2. Rear quarter view of external elevator balance test setup (University of Washington wind tunnel).

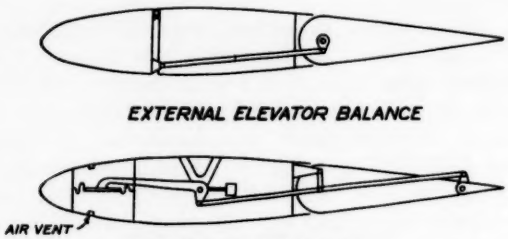

FIG. 3. Diagrammatic cross-sectional view of angle of attack balances tested, omitting for simplicity the means of adjusting the linkage.

DESCRIPTION OF TESTS MADE ON TWO TYPES OF ANGLE OF ATTACK BALANCES

External Elevator Balance

The first type of angle of attack balance was tested in the University of Washington wind tunnel in Seattle while the author was connected with this University. The model consisted of a N.A.C.A. 0009 airfoil having the forward portion hinged at the 30 per cent chord axis to form an external elevator balance surface. This surface was connected by mechanical means to a 35 per cent chord elevator such that a downward movement of the elevator caused a small upward angular movement of the external balance surface, which in effect meant that a fraction R of the hinge moment developed by the balance surface was transmitted to the elevator. A rear quarter view of the test setup showing the wire pulley arrangement for measuring elevator hinge moments is shown in Fig. 2. In Fig. 3 a diagrammatic sketch of the typical linkage is shown, but for simplicity the means of adjusting the links is not shown. The hinge gap of the balance surface was sealed at the center by a squeezed rubber tube, and a gap of 0.10 in. occurred at the airfoil surface for the balance surface in the undeflected position. The elevator gap was not sealed but was made small. Model dimensions are given in Table 1.

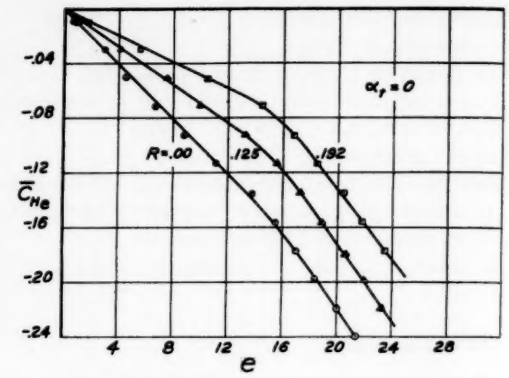

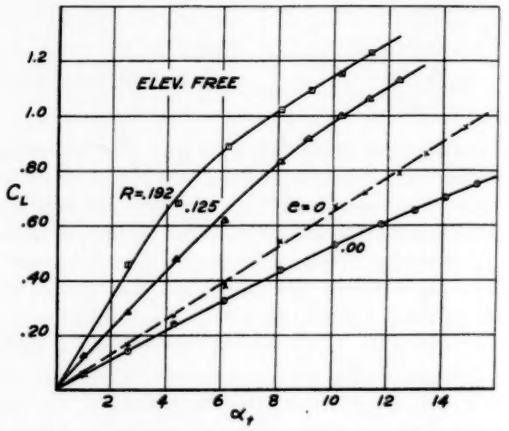

FIG. 4. Measured lift and hinge moment coefficients with external elevator balance.

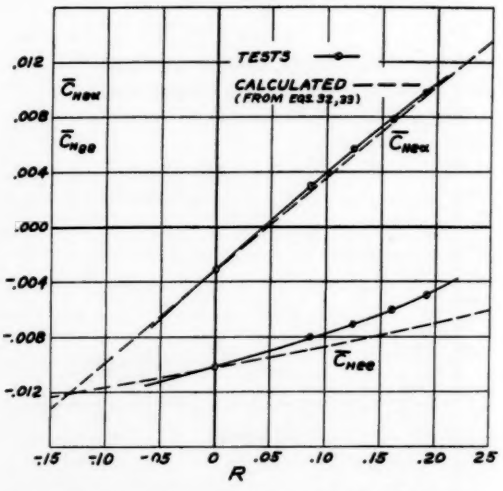

FIG. 5. Comparison of measured and calculated hinge moment coefficient derivatives for external elevator balance.

Some results of these tests are shown in Figs. 4 and 5. In Fig. 4 the elevator hinge moment, coefficient $\bar{C}_{He}$ for $\alpha_t = 0$, is plotted against elevator angle for different values of R. These curves are linear up to $e = 15°$ after which their slopes are constant. The lower curves show how the lift coefficient varies when the

TABLE 1
Model Dimensions

	External Elev. Bal. Model	Internal Tab Bal. Model
Wing span	36 in.	60 in.
Wing chord	15 in.	24.54 in.
Wing aspect ratio	2.4	2.79
Diameter of circular end plates	24 in.	36 in.
Elevator chord aft	5.25 in.	8.07 in.
Tab chord		2.0 in.
Tab span		42.0 in.
Balance effective moment arm or chord	4.50 in.	8.0 in.
Balance effective area	162 sq. in.	57 sq.in.

elevator is allowed to float downward. On this same curve the lift coefficient for $e = 0$ is plotted for comparison, along with the curve for a normal free elevator ($R = 0$). In Fig. 5 values of the hinge moment derivatives for different values of R are shown plotted along with calculated values of these parameters determined by the method presented in a later section of this paper. The maximum lift coefficients are not shown, but it was found that the effect of the movable nose balance for the value of R tested did not reduce the maximum angle of stall to any appreciable extent.

Internal Tab Balance

The second type of angle of attack balance was tested at the Massachusetts Institute of Technology and consisted of a N.A.C.A. 0010 airfoil having a 40 per cent chord elevator with a 20 per cent elevator chord tab having a span of 70 per cent of the elevator span. This tab was connected to an internal tab balance surface located inside the stabilizer in a typical but somewhat different manner to that shown in Fig. 3. The internal balance surface had a slack diaphragm seal with the regions on each side vented by a series of holes located in the metal airfoil surface. An adjustable means was provided to change the movement of this internal surface in relation to the tab movement. Elevator hinge moments were measured by use of electric strain gauges, and a fractional horsepower electric motor was provided to change the elevator angle without stopping the wind tunnel. Two autosyn indicators were used to measure the elevator and tab angles. Fig. 6 shows a detail view of the internal balance surface and autosyn angle transmitters. In this model the elevator, tab, and internal surface were carefully statically balanced. Model dimensions are given in Table 1.

Typical test results are shown in Figs. 7 and 8. In Fig. 7 the lift coefficient plotted against angle of attack for the elevator free is shown for the internal balance surface vented at 10 and 15 per cent of the airfoil chord for $R = -0.0426$. This shows that the tab effectively controls the elevator up to the limit of the tab which was near 30°. The maximum tab deflection

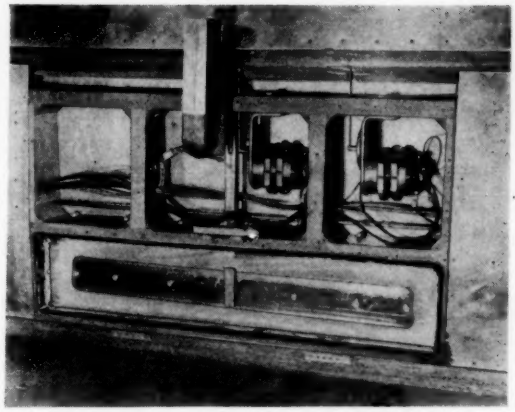

FIG. 6. Detailed view of internal tab balance showing elevator and tab angle autosyns.

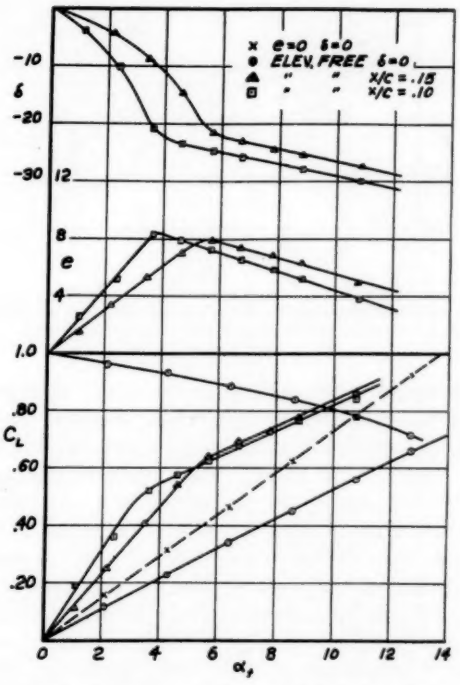

FIG. 7. Elevator free tests of internal tab balance for pressure vents at 10 and 15 per cent of chord ($R = -0.0426$).

varied to some extent because of restraints on the mechanical mechanism which changed for different elevator angles. In this same figure the corresponding elevator and tab angles are also plotted. In Fig. 8, curves of hinge moment coefficients for the elevator, with the tab floating in conjunction with the internal balance surface vented at the 10 per cent chord position, are shown along with the corresponding tab angles. In addition to these hinge moments, the pressure ratio P of the 10 per cent chord position is plotted against e for $\alpha_t = 0$. This pressure ratio agreed very well with the calculated pressures from Fig. 10 up to $e = 15°$, after which a drop in pressure gradient of about

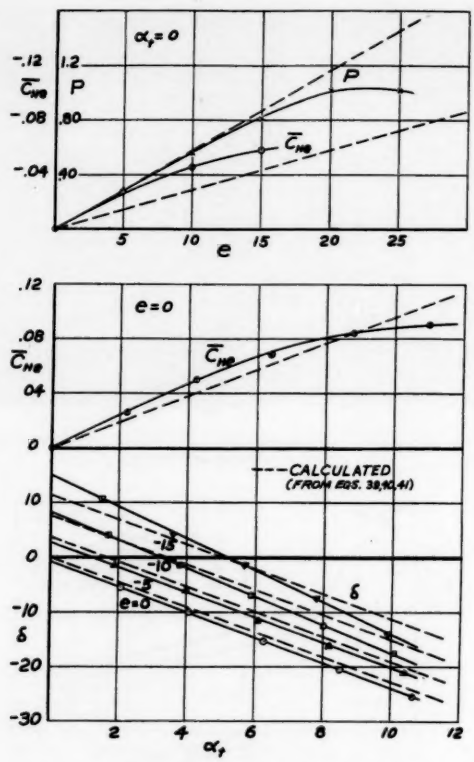

FIG. 8. Comparison of measured and calculated elevator hinge moment coefficients and table angles for internal tab balance with 10 per cent pressure vents ($R = -0.0426$).

50 per cent is to be expected. Fig. 8 also includes the calculated values of elevator hinge moments and tab angles as found from equations and charts presented in a later part of this paper. These calculations agreed very well except for the case of $\bar{C}_{He}$ vs. e. In this case the calculations indicated a greater reduction in hinge moment than did the tests, when $\alpha_t = 0$. A possible explanation of this may be that the pressures created by the deflecting tab modified the pressures at the 10 per cent chord position for the deflected elevator, the effect of which has not been included in the calculations.

METHOD OF PREDICTING HINGE MOMENTS FOR AN EXTERNAL ELEVATOR BALANCE

The first problem in predicting the effect of an external elevator balance forming the forward portion of the stabilizer is to calculate the hinge moment coefficients for such a hinged surface. This has been done by graphically integrating the pressures of Fig. 10 to form Fig. 9, which represents the hinge moment coefficients of the forward portion of an airfoil having two serially hinged flaps. The hinge moment coefficients of the external elevator balance C_{HN} have been based upon the elevator chord rather than the balance chord; hence, these coefficients may be added directly to the hinge moment coefficient for the elevator. The value of C_{HN} is given by the equation

$$C_{HN} = C_{HA}C_L + C_{HB\theta}\theta + C_{HBe}e \tag{29}$$

where

$$C_L = m_t(\alpha + k_\theta\theta + k_e e) \tag{30}$$

For the present analysis the angle of attack α_t of the horizontal tail is taken with respect to the fixed portion of the stabilizer and the angular movement of the external elevator balance θ_N is measured positive for an upward movement of the balance nose. Here the external elevator balance is assumed to transmit a fraction R of its hinge moment to the elevator which remains constant for all elevator angles; hence, the following relations may be substituted in Eqs. (29) and (30).

$$\alpha = \alpha_t + \theta_N$$

$$\theta = -\theta_N$$

$$\theta_N = Re$$

$$C_{He} = RC_{HN} \text{ (due to stabilizer balance)}$$

If this external balance surface hinge moment is added to that produced by the elevator the resulting hinge moment of the elevator system becomes

$$\bar{C}_{He} = \bar{C}_{He\alpha}\alpha_t + \bar{C}_{Hee}e \tag{31}$$

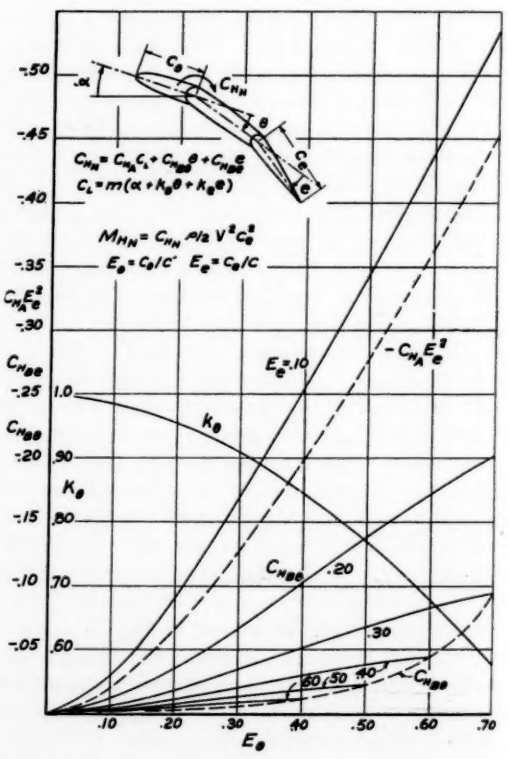

FIG. 9. Chart for calculating external elevator balance hinge moments.

where

$$\bar{C}_{H\epsilon\alpha} = C_{H\epsilon\alpha} + C_{HA}m_t R \tag{32}$$

$$\bar{C}_{H\epsilon\epsilon} = C_{H\epsilon\epsilon} + [C_{HA}k_e m_t + C_{HBe}]R + [C_{HA}m_t 1 - k_\theta) - C_{HB\theta}]R^2 \tag{33}$$

If m_{tf} is the slope of the tail lift coefficient curve for elevator free, then from Eqs. (30) and (31) for the condition that $\bar{C}_{He} = 0$

$$m_{tf} = m_t[1 + (1 - k_\theta)R + k_e]\bar{C}_{H\epsilon\alpha}/\bar{C}_{H\epsilon\epsilon} \tag{34}$$

These equations permit the necessary horizontal tail characteristics to be calculated for an external elevator balance and are generally valid up to $e = \pm 15°$.

Calculated values of $\bar{C}_{H\epsilon\alpha}$ and $\bar{C}_{H\epsilon\epsilon}$ have been made for the model tested using the above equations and the results plotted in Fig. 5. These calculations are based upon $C_{H\epsilon\alpha} = -0.0031$, $C_{H\epsilon\epsilon} = -0.0102$, $m_t = 0.064$, and $k_e = 0.59$ as found from wind-tunnel tests. Then using Fig. 9 for $E_\theta = 0.30$ and $E_e = 0.35$, the value of $C_{HA} = -(-0.128) \div (0.35)^2 = 1.045$, $C_{HB\theta} = -0.006$, $C_{HBe} = -0.026$, and $k_\theta = 0.91$.

Method of Predicting Hinge Moments for an Internal Tab Balance

In this section equations will be developed permitting the elevator hinge moments to be calculated for the case where a hinged surface within the stabilizer is connected to float freely in conjunction with an elevator tab.

The resultant air pressure acting on the internal surface for a one-degree change in α_t or e may be found from Fig. 10 for any pressure duct location (x/c). This figure has been calculated from reference (1) based upon characteristics for a sealed elevator. The pressure ratio difference acting on the internal surface S_θ is then

$$P = P_\alpha \alpha_t + P_e e \tag{35}$$

If c_θ is the distance of the center of pressure of this surface from its hinge and if R is the fraction of hinge moment developed by this surface that is transmitted to the tab, the tab hinge moment coefficient due to the internal surface will be

$$C_{H\delta} = (P_\alpha \alpha_t + P_e e)(S_\theta c_\theta / S_t c_t)R \tag{36}$$

Here a positive value of R will develop a tab hinge moment tending to deflect the tab to a positive value of δ. Combining the above equation with the normal tab hinge moment equation, the total tab hinge moment may be expressed as

$$C_{H\delta} = C_{H\delta\alpha}\alpha_t + C_{H\delta e}e + C_{H\delta\delta}\delta + (P_\alpha \alpha_t + P_e e)(S_\theta c_\theta / S_t c_t)R \tag{37}$$

The elevator hinge moment is

$$C_{He} = C_{He\alpha}\alpha_t + C_{Hee}e + C_{He\delta}\delta \tag{38}$$

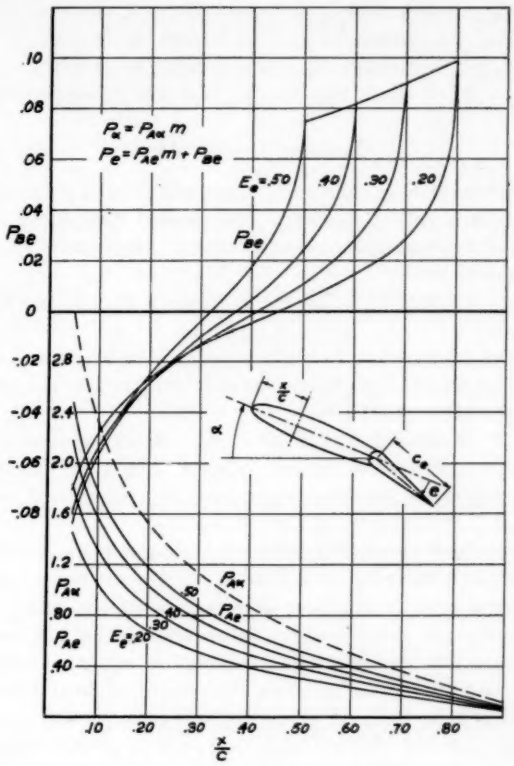

Fig. 10. Chart for calculating chord-wise pressure difference ratio for an airfoil with deflected flap.

By combining Eqs. 37 and 38 modified values of $C_{H\epsilon\alpha}$ and $C_{H\epsilon\epsilon}$ may be calculated which incorporates the effects of this floating tab. If these are denoted as $\bar{C}_{H\epsilon\alpha}$ and $\bar{C}_{H\epsilon\epsilon}$, then

$$\bar{C}_{H\epsilon\alpha} = C_{H\epsilon\alpha}\left[1 - \frac{C_{H\epsilon\alpha}C_{H\delta\alpha}}{C_{H\epsilon\alpha}C_{H\delta\delta}} - \frac{C_{H\epsilon\delta}P_\alpha}{C_{H\epsilon\alpha}C_{H\delta\delta}}\left(\frac{S_\theta c_\theta}{S_t c_t}\right)R\right] \tag{39}$$

$$\bar{C}_{H\epsilon\epsilon} = C_{H\epsilon\epsilon}\left[1 - \frac{C_{H\epsilon\delta}C_{H\delta e}}{C_{H\epsilon\epsilon}C_{H\delta\delta}} - \frac{C_{H\epsilon\delta}P_e}{C_{H\epsilon\epsilon}C_{H\delta\delta}}\left(\frac{S_\theta c_\theta}{S_t c_t}\right)R\right] \tag{40}$$

The tab position in terms of α_t and e may be written directly from Eq. (37) for $C_{H\delta} = 0$ giving,

$$\delta = -\left[\frac{C_{H\delta\alpha}}{C_{H\delta\delta}} + \frac{P_\alpha}{C_{H\delta\delta}}\left(\frac{S_\theta c_\theta}{S_t c_t}\right)R\right]\alpha_t - \left[\frac{C_{H\delta e}}{C_{H\delta\delta}} + \frac{P_e}{C_{H\delta\delta}}\left(\frac{S_\theta c_\theta}{S_t c_t}\right)R\right]e \tag{41}$$

Knowing the tab position as a function of α_t and e, the lift and hinge moments of the horizontal surface may be found for cases where the tab effectiveness reduces at the larger tab angles. This may be done by using wind-tunnel data obtained for various fixed tab settings. Calculated values of hinge moment coefficients and tab angles are shown in Fig. 8, based upon pressures from Fig. 10, and the following coefficients are determined from the wind-tunnel tests:

$C_{H\alpha\alpha} = -0.0048$ $C_{H\delta\alpha} = -0.0010$ $R = -0.0426$
$C_{H\alpha\epsilon} = -0.0090$ $C_{H\delta\epsilon} = -0.0010$ $k_e = 0.59$
$C_{H\alpha\delta} = -0.0075$ $C_{H\delta\delta} = -0.0097$ $m_t = 0.073$
$P_\alpha = 0.169$ (from Fig. 10), $P_\epsilon = 0.058$ (from Fig. 10)

General Discussion

Several points concerning the application of this type of control will be discussed. At present there seems to be three desirable control force characteristics—namely,

(a) Control forces should not exceed a given magnitude.

(b) Control forces should not reverse in direction, i.e., a pull should always be necessary to increase the airplane angle of attack.

(c) Motion of the control column should be positive, i.e., a pull on the control column should be accompanied by a rearward movement of the control column.

Of these three, characteristics (a) and (b) seem important; however, it is believed that (c) is not a vital necessity, since airplanes have been flown and reported satisfactory in cases where the control motion has been completely reversed, maintaining, however, positive control forces. In applying the present angle of attack balance, a reversal of control movement will occur when the elevator is forced to float in a positive direction. One method of preventing this, if it is found necessary to do so, would be to provide a fore-and-aft horizontal tail, one surface being large enough for the pilot to handle with desirable control forces and the other forming a special stabilizer having an adjustable angle of attack balance. For this arrangement, as the airplane c.g. is shifted such as to reduce or increase the static stability, the stabilizing surface may be regulated to maintain the initial stability, giving the same control characteristics over an extended c.g. range.

Another point of concern is the possibility of hunting of the airplane for elevator free when the airplane is unstable for elevator fixed.* This can only be studied by a careful dynamic analysis; but, if control friction forces are kept low and if a reasonable amount of angle of attack balance is always used along with proper damping from other parts of the airplane, this tendency should be avoided.

A third point to be mentioned concerns the effect of compressibility shock waves effecting the airfoil pressures for high-speed airplanes. The external elevator balance may give trouble on high-speed airplanes because of a change in pressure distribution and therefore will require a careful investigation. It should be remembered that only 10 or 20 per cent of these pressure effects will be transmitted to the elevator; hence, control forces may not be altered to any great extent. For the case of the internal tab balance it is believed that if sufficient damping action is provided, which may easily be done by restricting the area of the air vents, satisfactory results should be obtained at high speed. Another combination, not tested but one that may be found desirable for a high-speed airplane, would be to connect the internal balance to the elevator directly instead of to the tab. This would require a greater internal balance surface area, but for a reasonable amount of regulated control this would not be too large, provided the elevator had some initial aerodynamic balance.

It should be pointed out that other control surfaces may likewise use this type of balance to an advantage in which case either a fixed or adjustable linkage may be found desirable.

References

[1] Allen, H. J., *Calculation of the Chordwise Load Distribution over Airfoil Sections with Plain, Split or Serially Hinged Trailing-Edge Flaps*, N.A.C.A. T.R. No. 634, 1938.

[2] Haus, Fr., *Automatic Stability of Airplanes*, N.A.C.A. T.M. No. 695, 1932.

* The following statement is quoted from page 33 of reference 2: "Good results have been obtained with incidence stabilizing devices, which were tested on airplanes with very little or no stability and which enabled the pilot to fly with release controls."

Torsional and Aileron Flutter

ZBIGNIEW KRZYWOBLOCKI*
Polytechnic Institute of Brooklyn

SUMMARY

The aim of this paper is to find an approximate solution of the influence of various elements on the critical frequency in a binary system of torsional and aileron vibration. Assuming the system as a nonconservative one and taking into account the results obtained by von Kármán and Biot, the influence of the kind of material and wing shape and airfoil thickness on the torsional frequency is considered. It is to be noted that damping is not taken into account. The idea of "wing torsional rigidity" is introduced, being inversely proportional to the angle of twist at the end of the wing. The problem of influence of the kind of material, aspect ratio and span, wing taper and airfoil thickness on the torsional frequency is solved in a first approximation from the point of view of proportion. Finally, the influence of various materials of wing and aileron is taken into consideration. An attempt is made to solve this problem by the aid of the partial differential equation based on Newton's Law. The equation is applied to an oscillating rod and permits the first natural frequency of the oscillating rod to be found. Using the Membrane Analogy, the differential equation is applied to a tubular member. The results are checked by the aid of Rayleigh's Method. The following conclusions are drawn:

(a) With regard to the influence of the kind of material on the binary system of torsional and aileron vibration, the decisive factor is the ratio of modulus of rigidity to the specific weight. High values of this ratio are obtained for steel and magnesium alloys; wood has the lowest ratio.

(b) The influence of span and airfoil thickness are significant and the influence of wing taper is less important.

(c) When a tubular member consists of various materials, a decisive factor is also the ratio of the modulus of rigidity to the specific weight. The following combinations might be advantageous: aluminum alloy or magnesium alloy wing and steel aileron, spruce-plywood wing and metal aileron.

(d) Three different methods lead to the same result—that, from a system of torsional oscillation standpoint, the decisive factor is the ratio of the modulus of rigidity to the specific weight. The methods include the computations based on the magnitude of the torsional frequency given by von Kármán and Biot, the differential equation based on Newton's Law, and Rayleigh's Method.

(e) The results obtained cannot be applied directly to practice because of the fact that damping, an important factor from wing flutter point of view, was not taken into account.

SYMBOLS USED

T	= kinetic energy
K	= $I_W + m_a s^2$
N	= $m_a s w_a$
R	= $m_a i_a^2$
I_w	= moment of inertia of the wing about the elastic axis
m_a	= mass of the aileron
s	= distance between the wing elastic axis and aileron hinge axis (the two axes are assumed to be parallel)
w_a	= distance of the center of gravity of aileron from the hinge axis (positive if the center of gravity is behind the hinge axis)
i_a	= radius of gyration of aileron
$m_a i_a^2$	= moment of inertia of aileron about the hinge axis
p_w	= angular deflection of wing relative to direction of flight
p_a	= angular deflection of aileron relative to direction of flight
P_1, P_2	= generalized forces
c_{11}, c_{12}, c_{21}, c_{22}	= coefficients
k_w, k_a	= coefficients
ω	= torsional frequency of oscillation
ω_{11}	= torsional frequency of the system, when aileron mass is concentrated on the hinge axis
ω_{22}	= frequency of aileron oscillating around hinge
v	= flight speed
Θ	= angle of twist at end of wing
M_t	= torque
A	= area enclosed by the mean curve of the periphery
G	= modulus of elasticity in shear (modulus of rigidity)
r	= Poisson's ratio
δ	= wall thickness
s	= length of centerline of ring section
L	= length of wing (semispan)
τ	= shearing stress
$\tau_{max.}$	= ultimate shearing stress
Φ	= wing torsional rigidity
γ	= specific weight
λ	= aspect ratio = $L/_t = F/_t^2 = L/F^2$
a	= bottom side of "wing working section" having rectangular shape
b	= height of "wing working section"
t	= length of wing chord
F	= wing area (semispan)
i_w	= radius of gyration of wing
W_w	= weight of wing
W	= weight of airplane
k_1, k_2, k_s	= constants
n_A	= coefficient depending on kind of flight
K	= constant
L_d	= design load
t_1	= length of wing root chord
t_2	= length of wing tip chord
n	= t_1/t_2 = taper ratio
t_m	= length of intermediate chord
μ	= a/b—assumed to be inversely proportional to airfoil thickness
H	= thickness of wing airfoil
$\Theta(x,t)$	= angle of twist of section at distance x from the origin relative to the section at the origin
ψ	= twist per unit length
C	= constant depending on the shape and size of section of rod

Presented at the Aerodynamics Session, Eleventh Annual Meeting, I.Ae.S., New York, January 25–29, 1943.

* Fellow, Polytechnic Institute of Brooklyn.

I = moment of inertia of cross section of rod about the x-axis (centroidal moment of inertia)
g = acceleration due to gravity
t = time
ρ = $(\gamma/g)I$ = moment of inertia per inch length
c_1, c_2, c_3, c_4 = constants
ω_1 = the first natural frequency
l = length of rod
U = potential energy
Θ_0 = angle of twist at free end of rod

Introduction

From a possible combination of flexural-torsional and aileron oscillation probably the most critical is the case of torsional and aileron oscillation. Strictly speaking, the influence of wing and wing shape on oscillation refers more to the problem of pure torsional or flexural oscillation than to the case of binary system of torsional and aileron oscillation.

In the latter case an important factor is the influence of aerodynamic qualities of the airfoil and the elasticity of the control system. In practice there probably never is a pure case of torsional or flexural oscillation but chiefly a general case of flexural-torsional and aileron oscillation. For this reason the author gives main consideration to the case of the binary system of torsional and aileron oscillation.

The Influence of Constructional Material and Shape of Wing

Basic Assumptions

In the following the wing is represented by a rigid cylindrical body, having a streamline section that is elastically restrained to the wing elastic axis. The wing is clamped to the airplane fuselage, which is considered a rigid base. The aileron is hinged at the aileron axis. Special attention is paid to the case of torsional oscillation of wing combined with oscillation of the aileron, because, as is known, this vibration is usually more effective in its results on account of the change of angle of attack.

The kinetic energy of the wing-aileron system can be expressed in the form:

$$T = (K\dot{p}_w^2 + 2N\dot{p}_w\dot{p}_a + R\dot{p}_a^2)/2 \tag{1}$$

Assuming the system as a nonconservative one, the moments as the generalized forces, and the angular deflections as the generalized coordinates

$$P_1 = -c_{11}p_w - c_{12}p_a \tag{2}$$

$$P_2 = -c_{21}p_w - c_{22}p_a \tag{3}$$

$c_{11}p_w$ represents the restoring moment about the wing elastic axis produced by an angular deflection of the wing. Its magnitude depends on the torsional stiffness of the wing and on the aerodynamic moment caused by a change of angle of attack.

$c_{12}p_a$ represents the moment about the wing elastic axis caused by the aileron deflection.

$c_{21}p_w$ represents the hinge moment caused by the change of wing's angle of attack.

$c_{22}p_a$ represents the hinge moment caused by the change of angle of attack of the aileron.

The system is nonconservative because:

$$c_{12} \neq c_{21} \tag{4}$$

Substituting the above equations in Lagrange's equations

$$K\ddot{p}_w + N\ddot{p}_a = -c_{11}p_w - c_{12}p_a \tag{5}$$

$$N\ddot{p}_w + R\ddot{p}_a = -c_{21}p_w - c_{22}p_a \tag{6}$$

Substituting

$$p_w = k_w e^{i\omega t} \tag{7}$$

$$p_a = k_a e^{i\omega t} \tag{8}$$

$$\omega_{11}^2 = c_{11}/K \tag{9}$$

$$\omega_{22}^2 = c_{22}/R \tag{10}$$

and assuming that $w_a = 0$—i.e., that the center of gravity of the aileron lies on the hinge axis, that the aileron is statically balanced, and that there is no dynamic coupling between the coordinates p_w and p_a—von Kármán and Biot[1] obtained the following condition for the stability of the system:

$$\omega^2 = \frac{\omega_{11}^2 + \omega_{22}^2}{2} \pm \sqrt{\left(\frac{\omega_{11}^2 + \omega_{22}^2}{2}\right)^2 - \omega_{11}^2\omega_{22}^2 + \frac{c_{12}c_{21}}{KR}} \tag{11}$$

The system is stable only if ω is real—i.e., ω^2 is real and positive. To accomplish this there are two conditions:

$$\frac{\omega_{11}^2 + \omega_{22}^2}{2} > \sqrt{\left(\frac{\omega_{11}^2 + \omega_{22}^2}{2}\right)^2 - \omega_{11}^2\omega_{22}^2 + \frac{c_{12}c_{21}}{KR}} \tag{12}$$

and

$$\left(\frac{\omega_{11}^2 + \omega_{22}^2}{2}\right)^2 - \omega_{11}^2\omega_{22}^2 + \frac{c_{12}c_{21}}{KR} > 0 \tag{13}$$

or

$$(\omega_{11}^2 - \omega_{22}^2)^2 + 4(c_{12}c_{21}/KR) > 0 \tag{14}$$

Usually the product of c_{12} and c_{21} is less than zero. ω_{11}^2 should be as large as possible. The system is unstable in the neighborhood of $\omega_{11} = \omega_{22}$. The case $w_a \neq 0$ is not taken into consideration because the results obtained will not be changed in that case. Both ω_{11} and ω_{22} depend on the flight speed; the coefficient c_{11} and the torsional frequency ω_{11} decrease with the flight speed; the frequency ω_{22} increases with the speed.

At a certain speed these two frequencies will, of course, coincide.

Wing-Torsional Rigidity

All four coefficients c_{11}, c_{12}, c_{21}, c_{22} given above depend on the aerodynamic properties of the wing and the aileron. Besides this, only one coefficient, c_{11}, depends on the constructional properties of the wing. To consider the influence of the wing material and wing shape on the torsional frequency ω_{11} the influence of the above-mentioned elements on this frequency must be taken into account. To accomplish this and to avoid complicated computations, the problem will be considered from a qualitative and not from a quantitative point of view. To do this, the conception of proportionality instead of the conception of equality is introduced.

Torsional rigidity is usually the factor by which the torque is divided to obtain the twist per unit length. In these considerations another element introduced concerns the torsional rigidity of an airplane wing. In wing construction the most important consideration is perhaps the angle of twist at the end of the wing. Wing twisting causes a change of aerodynamic qualities. In many countries the aircraft requirements often limit this angle to a certain value, mostly 2°. As the measure of the "wing torsional rigidity" unity divided by the greatness of this angle is accepted. Using Bredt's equation for a thin tubular section

$$\Theta = \int_0^L \frac{M_t}{4A^2G} \oint \frac{ds}{\delta}\, dl \tag{15}$$

This equation can be modified to

$$M_t = 2A\delta\tau \tag{16}$$

or

$$M_t = 2A\delta\tau_{max.} \tag{17}$$

Substituting Eq. (17) in Eq. (15) and assuming, for comparison, $\delta = a$ constant:

$$\Theta = \int_0^L \frac{\tau_{max.}}{2AG} \oint ds\, dl \tag{18}$$

As the wing torsional rigidity, it is assumed that

$$\Phi = 1/\Theta \tag{19}$$

The Influence of the Kind of Material

It is assumed that: (a) the aerodynamic properties of the wing are the same (λ, airfoil, and chord); (b) the shape and construction of wing are the same; (c) the change of material does not affect the values A, s, and the radius of gyration of the wing; and (d) damping is not taken into account.

Using these assumptions

$$\Phi = \text{const.}\ \frac{G}{\tau_{max.}} \sim \frac{G}{\tau_{max.}} \tag{20}$$

From Eq. (9)

$$\omega_{11}^2 = \frac{c_{11}}{K} = \frac{c_{11}}{I_w + m_a s^2} \tag{21}$$

It is known that the restoring moment $c_{11}p_w$ corresponds to the torsional rigidity of the wing and to the aerodynamic moment caused by a change of angle of attack. In the first approximation, not considering the degree of proportionality, only the torsional rigidity and weight of the wing can be taken into account.

$$\omega_{11}^2 = \text{const.}\ \frac{\Phi}{I_w} = \text{const.}\frac{\Phi}{W_w} \sim \frac{\Phi}{W_w} \tag{22}$$

The weight of the wing is proportional to δ and γ. From Eq. (17) the assumption that M_t = const. and A = const. gives

$$\delta = \text{const.}\ \frac{1}{\tau_{max.}} \sim \frac{1}{\tau_{max.}} \tag{23}$$

Substituting Eqs. (20) and (23) in Eq. (22) gives:

$$\omega_{11}^2 = \text{const.}\ \frac{G}{\gamma} \sim \frac{G}{\gamma} \tag{24}$$

Therefore, in considering the influence of the kind of material on the binary system of torsional and aileron oscillation, the decisive factor is the ratio of modulus of rigidity to the specific weight. The values of this ratio, given in Table 1, are taken from references 2 and 6.

TABLE 1

Kind of Material	Modulus of Rigidity, G, Lbs. per Sq.In.	Specific Weight, γ, Lbs. per Cu.In.	$\frac{G}{\gamma} \times$ 10,000	Ultimate Shear Stress, $\tau_{max.}$ Lbs. per Sq.In.	$G/\tau_{max.}$
Spruce	84,000	0.0157	536	1,000	84
Spruce-plywood 45°	420,000	0.0188	2,235	2,370	177
Mild 1025 steel	11,000,000	0.2833	3,890	35,000	314
C.M. steel	11,000,000	0.2833	3,890	55,000	200
17ST aluminum-Alloy sheet	3,800,000	0.1010	3,760	33,000	115
Magnesium alloys*	2,500,000	0.0660	3,790	18,000	139
Duramold†	.....	....	3,380	....	..

*According to reference 6 the modulus of elasticity of magnesium alloys is 6,500,000 lbs. per sq.in. Assuming $G = E/2(1 + r)$ and $r = 0.3$ the above given value is obtained. To obtain $\tau_{max.}$ for magnesium alloys it is assumed that

$$\tau_{max.} \leqq 0.6 \times \text{ultimate tensile stress}$$

This ratio in a first approximation is in agreement for the metals used; according to references 6 and 7 the ultimate tensile stress for magnesium alloy structural shapes equals 30,000 lbs. per sq.in.

† According to reference 12 tests for Duramold show:

$$3{,}060 = E/1{,}000 \times \text{specific gravity}$$

and as

$$\text{Specific gravity} = 1{,}728 \times \text{specific weight}/62.5$$

Assuming

$$G = E/2(1 + r),\ r = 0.25$$

one has

$$\frac{G}{\text{specific weight}} = \frac{3{,}060{,}000 \times 1{,}728}{62.5 \times 2.5} = 3{,}380 \times 10^4$$

The value obtained presents only the first approximation and the results should perhaps be used cautiously.

As is seen, metals have a greater ratio of G/γ in comparison with wood, even plywood. The high value of magnesium alloys is interesting, as is that of Duramold.

If, in a special case, it is assumed that the weight of the wing is constant Eqs. (20) and (22) give

$$\omega_{11}^2 = \text{const. } \Phi \sim \frac{G}{\tau_{max.}} \tag{25}$$

Eq. (25) is in agreement with Eq. (4: 70) given by Younger.[7] Some values of this ratio are given in Table 1. Again the great advantage of metal is seen, especially steel, in comparison to ordinary wood. The high value obtained for plywood is striking.

The Influence of Aspect Ratio and Span

Assume that (a) the airfoil section and wing surface area are constants; (b) the shape of the wing is rectangular; (c) the geometric details of construction are the same regardless of the materials; (d) the spar or "working section" of the wing is a rectangular shell having lower side a, height b, and a uniform thickness of walls δ; (e) the side a is proportional to length of chord; (f) the height b is proportional to thickness of profile and also to length of chord (thickness is accepted as a percentage of chord length).

For comparable aims Eq. (18) may be modified to take into account an intermediate section, approximately in the center of the wing span. This assumption and the equalities

$$\oint ds = s \cong 2\,(a + b) \tag{26}$$

$$A \cong ab \tag{27}$$

permit the writing of

$$\Theta \cong \frac{\tau_{max.}\ (a + b)L}{abG} \tag{28}$$

where a and b refer to the accepted intermediate section. As

$$\begin{aligned} a &= \text{const. } t \sim t \\ b &= \text{const. } t \sim t \end{aligned} \tag{29}$$

therefore

$$(a + b) = \text{const. } t \sim t \tag{30}$$

$$ab = \text{const. } t^2 \sim t^2 \tag{31}$$

$$\Theta = \text{const. } \frac{L}{t} \sim \frac{L}{t} = \lambda = \frac{L^2}{F} \sim L^2 \tag{32}$$

$$\Phi = \text{const. } 1/\lambda = \text{const.}/L^2 \sim 1/L^2 \tag{33}$$

Modifying Eq. (21)

$$\omega_{11}^2 = \frac{c_{11}}{I_w + m_a s^2} = \text{const. } \frac{\Phi}{I_w} \sim \frac{\Phi}{I_w} \tag{22}$$

the change of I_w must be taken into account. Assuming that the distance measured along the wing chord line is proportional to the length of the chord line gives

$$i_w^2 = \text{const. } t^2 \sim (1/L^2) \tag{34}$$

There are various formulas expressing the change in wing weight with change of span. For instance, in reference 3

$$\frac{W_w}{F} = \left(k_1 + k_2 \frac{L^2}{F}\right) n_a L \frac{W}{F} + k_z \tag{35}$$

In reference 4

$$W_w = K \frac{\lambda L_d F}{1{,}000t} \tag{36}$$

or

$$W_w = K \frac{F^2 \times L_d}{1{,}000t^3} \tag{37}$$

It is seen that as a first approximation[5]

$$W_w = \text{const. } L^3 \sim L^3 \sim \frac{1}{t^3} \tag{38}$$

Therefore

$$I_w \sim W_w \times i_w^2 \sim L \sim \frac{1}{t} \tag{39}$$

Substituting Eqs. (33) and (39) in Eq. (22):

$$\omega_{11}^2 \sim \frac{\Phi}{I_w} \sim \frac{1}{L^3} \sim t^3 \tag{40}$$

It can be seen that the influence of span on the binary system of torsional and aileron vibration is significant. The author obtained similar results by a graphic method.[5]

The Influence of Wing Taper

The assumptions are: (a) the aerodynamic profile and area of wing are the same; (b) the construction and material of wing are the same; (c) the plan form of the wing is a trapezoid; (d) the length of the wing root chord t_1 is constant; other assumptions are similar to those applied above.

It follows that

$$t_1 = nt_2 \tag{41}$$

$$F = Lt_m = \text{constant} \tag{42}$$

$$t_m = \frac{t_1 + t_2}{2} = \frac{t_1[1 + (1/n)]}{2} \tag{43}$$

$$L = F/t_m = \text{const. } \frac{1}{1 + (1/n)} \sim \frac{1}{1 + (1/n)} \tag{44}$$

Substituting Eq. (44) in Eq. (40) gives

$$\omega_{11}^2 = \text{const. } [1 + (1/n)]^3 \sim [1 + (1/n)]^3 \tag{45}$$

The function

$$L = f(n) \tag{46}$$

has a horizontal asymptote. It is seen that the influence of taper is greater for smaller values of n and less when n increases. When two wings are compared, one rectangular and the other trapezoidal, having the same wing area, the results show that (a) assuming the same value of λ and changing l_1 and l_2, both wings are equivalent from the standpoint of ω_{11}; (b) assuming the same length of wing root chord, the trapezoidal wing is less advantageous than the rectangular one (because λ is greater).

The Influence of Airfoil Thickness

The assumption is made that the only dimensional variable is the thickness of airfoil and that the height b of the working section is proportional to the thickness. Modifying Eq. (28):

$$\theta = \text{const.}\frac{a+b}{ab} = \text{const.}\frac{a[1+(1/\mu)]}{a^2(1/\mu)} \sim \mu + 1 \tag{47}$$

Therefore, since a is always large in comparison to b

$$\theta \sim \mu \tag{48}$$

Assuming that the weight of wing is affected by the change of airfoil thickness in the manner given by Younger[7] [Eq. (4: 40)]—i.e., that the wing weight is inversely proportional to the thickness of the wing,

$$W_w = \text{const.}\frac{1}{H} \sim \frac{1}{H} \tag{49}$$

μ is inversely proportional to the airfoil thickness. Substituting Eqs. (19), (48), and (49) in Eq. (22)

$$\omega_{11}^2 \sim \frac{H}{\mu} \sim H^2 \tag{50}$$

A significant influence of airfoil thickness is seen especially when taking into consideration the tendency to use thin airfoils on modern airplanes.

The Influence of Various Materials on Wing and Aileron

In practice, the wing frame sometimes consists of various materials—for instance, dural and steel. Also, different materials are used for wing and aileron, stabilizer and elevator, fin and rudder.

In a binary system of torsional and aileron oscillation, probably the deflections of the ailerons around the hinge line as a whole are more important than the torsional deflection of the aileron in itself. But one can imagine that the aileron is not free and that the elastic restraints such as control wires are not flexible enough. On the assumption that one applies the irreversibility of aileron controls, the wing-aileron system can be treated as one unit. In the design office, the opinion is sometimes held that the same material for both parts increases the possibility of wing flutter. In other cases the possibility of wing flutter is more remote. In the case of the same material the parts are "in phase" and in another case "out of phase" from the wing oscillation standpoint. Evidently the "critical torsional frequency" of the system is removed in the second case to a higher value.

In an attempt to solve this problem the torsional oscillation of a rod fixed at one end and free at the other will first be considered. Newton's Law will be applied to obtain partial differential equation of the motion. Damping is not taken into account.

Assuming that the x-axis is taken along the centers of inertia of the cross sections of the rod, that there is pure torsion in each element of the rod, and that the section at distance x from the origin is twisted through the angle $\theta(x,t)$ relative to the section at the origin, where ω denotes the angular velocity of this section, an element of length δx is twisted through the angle $\delta\theta(x,t)$. The twist per unit length of this element is

$$\psi = \partial\theta(x,t)/\partial x \tag{51}$$

If M_t denotes the torque in this element[8]

$$M_t = CG\psi \tag{52}$$

The constant C depends on the shape and size of the section of rod and possesses the dimensions of the moment of inertia of an area. Assuming that I denotes the moment of inertia of the cross section of rod about the x-axis, the moment of inertia of the element of the rod of length δx is

$$(\gamma/g)I\delta x \tag{53}$$

The angular momentum of this element is

$$(\gamma/g)I\omega\delta x \tag{54}$$

The rate of increase of the angular momentum is equal to the total torque on the element. The total torque is the excess of the torque at $(x + \delta x)$ over that at x, also:

$$(\partial M_t/\partial x)\delta x \tag{55}$$

and

$$\frac{\partial}{\partial t}((\gamma/g)I\omega\delta x) = \frac{\partial M_t}{\partial x}\delta x \tag{56}$$

$$(\gamma/g)I\frac{\partial\omega}{\partial t}\delta x = \frac{\partial M_t}{\partial x}\delta x \tag{57}$$

Taking into account Eqs. (51) and (52)

$$\rho\frac{\partial^2\theta(x,t)}{\partial t^2} = CG\frac{\partial^2\theta(x,t)}{\partial x^2} \tag{58}$$

This equation is in accordance with methods given in references 8 and 9. The variable in this case is the angle of twist $\theta(x,t)$. Assuming that the rod vibrates harmonically at some natural frequency

$$\theta(x,t) = \theta(x)\sin\omega t \tag{59}$$

$$\frac{\partial^2\Theta(x,t)}{\partial t^2} = \left\{ - \Theta(x)\omega^2 \sin \omega t \right\} \tag{60}$$

$$\frac{\partial^2\Theta(x,t)}{\partial x^2} = \frac{d^2\Theta(x)}{dx^2} \sin \omega t \tag{61}$$

Substituting Eqs. (60) and (61) in (58)

$$\rho\Theta(x)\omega^2 + CG \frac{d^2\Theta(x)}{dx^2} = 0 \tag{62}$$

or

$$\frac{d^2\Theta(x)}{dx^2} + \frac{\rho\omega^2}{CG} \Theta(x) = 0 \tag{63}$$

This is an ordinary differential equation of the second degree. The general solution is

$$\Theta(x) = c_1 \sin x \sqrt{\frac{\rho\omega^2}{CG}} + c_2 \cos x \sqrt{\frac{\rho\omega^2}{CG}} \tag{64}$$

Assuming that the function

$$\Theta(x) = f(x) \tag{65}$$

is a quarter sine wave leads to the end conditions

$$x = 0, \qquad \Theta(x) = 0 \tag{66}$$

$$x = l, \; d\Theta(x)/dx = 0 \tag{67}$$

From the first condition,

$$c_2 = 0 \tag{68}$$

$$\Theta(x) = c_1 \sin x \sqrt{\frac{\rho\omega^2}{CG}} \tag{69}$$

The second condition gives

$$\frac{d\Theta(x)}{dx} = c_1 \sqrt{\frac{\rho\omega^2}{CG}} \cos l \sqrt{\frac{\rho\omega^2}{CG}} = 0 \tag{70}$$

or

$$\lambda \sqrt{\frac{\rho\omega^2}{CG}} = \pi/2, \, 3\pi/2, \, 5\pi/2 \ldots . \tag{71}$$

The first natural frequency

$$\omega_1 = \frac{\pi/2}{l} \sqrt{\frac{CG}{\rho}} \tag{72}$$

Applying this to a thin tube or to the case when the cross section of a tubular member has more than two boundaries, by use of Eqs. (146) and (162) in reference 11, one can write, on the basis of the Membrane Analogy:

$$M_t = \int \frac{4A^2G}{ds} \psi\delta \tag{73}$$

It is seen that in a first approximation Eq. (52) can be modified to

$$M_t = \psi \int \frac{4A^2G}{ds} \delta \tag{74}$$

Therefore the expression for CG in Eq. (52) becomes

$$\int (4A^2G/ds)\delta \tag{75}$$

However, the thickness δ is inversely proportional to the maximum allowable stress $\tau_{max.}$. Thus, Eq. (74) becomes

$$M_t = c_3\psi \int \frac{A^2}{ds} \frac{G}{\tau_{max.}} \tag{76}$$

Assuming that the dimensions of the wing are unchanged

$$M_t = c_4\psi \int \frac{G}{\tau_{max.}} \tag{77}$$

Let it be assumed that the tubular member consists of various materials, ideally connected together. In computing the first natural frequency of this system, Eq. (72) can be applied substituting instead of CG the expression

$$c_4 \int \frac{G}{\tau_{max.}} = c_4 \sum_{i=1}^{i=n} \frac{G_i}{\tau_{max.i}} \tag{78}$$

where the subscript i refers to various materials.

Similarly, Eq. (53) can be modified. So instead of

$$(\gamma/g) \, I \, \delta x \tag{53}$$

the following expression may be introduced:

$$[(\gamma_1/g)I_1 + (\gamma_2/g)I_2 + \ldots . (\gamma_n/g)I_n]\delta x = \left[\sum_{i=1}^{i=n} (\gamma_i/g)I_i\right]\delta x \tag{79}$$

if $\gamma_1, \gamma_2, \ldots . \gamma_n$, refer to the first material, second material, and so on, and $I_1, I_2 \ldots . I_n$ signify the partial moment of inertia of the parts of the tubular member made from the first and second material, etc. The value I_n in a tubular member is proportional to the corresponding wall thickness δ, which is in turn inversely proportional to $\tau_{max.}$ Therefore

$$\sum_{i=1}^{i=n} (\gamma_i/g)I_i = \text{const.} \sum_{i=1}^{i=n} \frac{\gamma_i}{\tau_{max.i}} \tag{80}$$

In computing the first natural frequency of torsional oscillation of a tubular member consisting of various materials, one must use instead of Eq. (72) the equation:

$$\omega_1 = \frac{\pi/2}{l} \text{const.} \sqrt{\sum_{i=1}^{i=n} \frac{G_i}{\tau_{max.i}} : \sum_{i=1}^{i=n} \frac{\gamma_i}{\tau_{max.i}}} = \frac{\pi/2}{l} \text{const.} \sqrt{\sum_{i=1}^{i=n} \frac{G_i}{\gamma_i}} \tag{81}$$

In practice a wing and an aileron do not represent a rigidly connected system as the one assumed in the

above given computation, because the wing-aileron system is an elastically connected one. However, the above given computations give an approximate idea with regard to the "critical torsional frequency" of a system consisting of various materials.

It can be seen that the frequency ω_1 is influenced by a selection of materials having different ratios of G/γ. Table 1 shows that such combinations as plywood and steel or aluminum alloys and steel might be advantageous. In practice, these combinations are applied. The result, obtained above, can be verified by Rayleigh's Method. In any free vibration the following condition must be realized:[10]

(Total kinetic energy) + (Total potential energy) = Const. (independent of t) (82)

In other words, this condition may be expressed in the following:

maximum potential energy = maximum kinetic energy (83)

The energies of the oscillation rod (torsional oscillation), having circular cross section will be computed.

The total potential energy stored in a slide dx of the rod can be expressed:

$$dU = M_t^2 dx/2GI \tag{84}$$

From Eq. (52)

$$M_t = IG \frac{\partial \Theta(x,t)}{\partial x} \tag{52a}$$

The maximum potential energy occurs in the most deflected position. Taking that moment into consideration, it is seen that Θ will be independent of t (time). One has to assume a shape for the first normal deflection curve, i.e., angle Θ versus distance x. As before, a quarter sine or cosine wave may be assumed. Choosing

$$\Theta(x,t) = \Theta(x) = \Theta_0 \sin \frac{\pi x}{2l} \tag{85}$$

remembering that

$$\frac{\partial \Theta(x,t)}{\partial x} = \frac{d\Theta(x)}{dx} = \Theta_0 \frac{\pi}{2l} \cos \frac{\pi x}{2l} \tag{86}$$

and substituting Eqs. (52a) and (83) in Eq. (87)

$$U = \int_0^l \frac{M_t^2 \, dx}{2GI} \tag{87}$$

gives

$$U = \frac{1}{16l} GI\Theta_0^2 \pi^2 \tag{88}$$

The maximum kinetic energy occurs in the undeformed position where the velocity is greatest. The kinetic energy of a rod element dx is:

$$dT = (\rho/2)\, \dot{\Theta}^2(x,t)\, dx \tag{89}$$

But

$$\dot{\Theta} = \omega\Theta(x,t) \tag{90}$$

Substituting Eq. (85) into Eq. (89) and integrating

$$T = \int_0^l \frac{\rho\omega^2}{2} \Theta_0^2 \left(\sin \frac{\pi x}{2l}\right)^2 dx \tag{91}$$

After integration

$$T = \rho l \omega^2 \Theta_0^2/4 \tag{92}$$

From the condition

$$T = U \tag{93}$$

one has

$$\omega = \omega_1 = \frac{\pi/2}{l} \sqrt{\frac{GI}{\rho}} \tag{94}$$

Eq. (94) is identical with Eq. (72).

The assumed function does not fulfill satisfactorily the required end conditions. The assumed curve must be horizontal at $x = 0$ and the angle of twist at the free end must be equal Θ_0. The following equation satisfies these conditions:

$$\Theta(x) = \Theta_0 \left(1 - \cos \frac{\pi x}{2l}\right) \tag{85a}$$

This function does not present in the present case an approximation of a high degree. The result is:

$$U = \frac{1}{16l} GI\Theta_0^2 \pi^2 \tag{88a}$$

$$T = [(3/4) - (2/\pi)]\rho l \omega^2 \Theta_0^2 \tag{91a}$$

$$\omega_1 \cong \frac{0.74\pi}{l} \sqrt{\frac{IG}{\rho}} \tag{94a}$$

Another curve may be assumed, but since this problem has been treated from a general point of view, this will not be discussed any further.

When applying the above method to a thin tube or to a tubular member having more than two boundaries, Eq. (73) instead of (52a) should be substituted. The same result would be obtained as formerly. Of course, in any given case it is necessary to take into account the change of I and ρ along the span. This will have an influence on the value of U and T.

Conclusions

The following conclusions may be noted:

(1) As far as the influence of the material on the binary system of torsional and aileron vibration, neglecting damping, is concerned, the decisive factor is the ratio of modulus of rigidity to the specific weight.

(2) In connection with (1) the following materials might be used, listed in the order from the most to the least advantageous: steel, magnesium alloys, 17ST

aluminum-alloy sheet, Duramold, spruce-plywood 45°, spruce.

(3) In a special case, assuming that the weight of wing of various materials is constant, the decisive factor in the binary system of torsional and aileron vibration is the ratio of modulus of rigidity to the ultimate shearing stress.

(4) In connection with (3) the materials might be listed in the following order: 1025 steel, C.M. steel, spruce-plywood 45°, magnesium alloys, 17ST aluminum-alloy sheet, spruce.

(5) Worthy of note are the high values obtained for steel in comparison to other materials.

(6) From (2) it can be seen that magnesium alloys might be advantageous and that plywood is less advantageous. Duramold is better than plywood.

(7) 17ST aluminum-alloy sheet has an average value from a torsional aileron vibration standpoint.

(8) The influence of span is significant, the square of the torsional frequency of the system being inversely proportional to the cube of the span.

(9) The influence of taper is greater for smaller values of taper ratio and less for greater values.

(10) The influence of airfoil thickness is also significant, the torsional frequency being proportional to the thickness.

(11) When a tubular member consists of various materials, the decisive factor is again the ratio of modulus of rigidity to the specific weight. (Damping is not taken into account.)

(12) In connection with (11) the materials might be listed as follows: steel, magnesium alloy, 17ST aluminum-alloy sheet, Duramold, spruce-plywood 45°, spruce.

(13) From the above it may be seen that the following combination might be advantageous: wing covered by 17ST aluminum sheet or by magnesium-alloy sheet—C.M. steel or 1025 steel aileron; wing covered by spruce-plywood 45°—C.M. steel, 1025 steel or 17ST aluminum alloy sheet aileron.

(14) From standpoint of torsional vibration the decisive factor is the ratio of the modulus of rigidity to the specific weight when damping is not taken into account.

(15) It is characteristic that the last conclusion is based on three different methods: i.e., the computation of the torsional frequency given by von Kármán and Biot, by Newton's Law, and by Rayleigh's Method. All lead to the same result.

(16) The above results cannot be applied directly in practice, because damping, an important factor from wing flutter point of view, was not taken into account. Damping probably would change the above results considerably.

References

[1] von Kármán, Theodore, and Biot, Maurice A., *Mathematical Methods in Engineering;* McGraw-Hill Book Company, Inc., New York and London, 1940.

[2] ANC-5, *Strength of Aircraft Elements,* Army-Navy-Civil Committee on Aircraft Requirements; U.S. Government Printing Office, Washington, D.C., 1938.

[3] Göthert, B., *Einfluss von Flächenbelastung, Flügelstreckung und Spanweitenbelastung auf die Flugleistungen,* Luftfahrtforschung, Bd. 16, Lfg. 5, May 20, 1939.

[4] Warner and Johnston, *Aviation Handbook;* McGraw-Hill Book Company, Inc., New York and London, 1931.

[5] Krzywoblocki, Zbigniew L., *The Influence of Span on Wing Flutter,* Aircraft Engineering, Vol. XIII, March, 1941.

[6] *Metals Handbook,* 1939 Edition; American Society for Metals, Cleveland, O.

[7] Younger, John E., *Mechanics of Aircraft Structures;* McGraw-Hill Book Company, Inc., New York and London, 1942.

[8] Prescott, John E., *Applied Elasticity;* Longmans, Green & Co., London, 1924.

[9] Den Hartog, J. P., *Mechanical Vibrations;* McGraw-Hill Book Company, Inc., New York and London, 1940.

[10] Southwell, R. V., *Theory of Elasticity;* Oxford, Clarendon Press, 1936.

[11] Timoshenko, S., *Theory of Elasticity;* McGraw-Hill Book Company, Inc., New York and London, 1934.

[12] Nichols, W., *Plastics and Aircraft,* Flight, Nos. 1760 and 1761, September 17 and 24, 1942.